UNIVERSITY OF OKLAHOMA

GRADUATE COLLEGE

VISCOSITY OF SHALE GAS

A THESIS

SUBMITTED TO THE GRADUATE FACULTY

in partial fulfillment of the requirements for the

Degree of

MASTER OF SCIENCE

By

HUY QUANG TRAN
Norman, Oklahoma
2017

VISCOSITY OF SHALE GAS

A THESIS APPROVED FOR THE
MEWBOURNE SCHOOL OF PETROLEUM AND GEOLOGICAL ENGINEERING

BY

_____
Dr. Ahmad Sakhaee-Pour, Chair

_____
Dr. Mashhad Fahs

_____
Dr. Zulfiquar Reza

Dedication

To my parents, Thang Tran and Ha Le, for their endless love, to my grandparents, Chuan Le and Suong Ha, for their encouragement, to my sister My Tran for her constant support.

Acknowledgements

First and foremost, I would like to express my deepest gratitude to Professor Ahmad Sakhaee-Pour, for his continuous support and motivation during my Masters study. The instructive weekly meetings equipped me with in-depth analysis and understanding of pore-structure, especially the acyclic pore-model. Dr. Sakhaee-Pour also encouraged me to consider problems from different perspective. Furthermore, his valuable comments on my research are always the most important part for me to improve myself. My research would not be possible without the help from Professor Ahmad Sakhaee-Pour.

To the members of my thesis committee, Dr. Reza and Dr. Fahs, I am truly grateful for your comments and assistances during my thesis defense. I am also forever in debt to the Mewbourne School of Petroleum and Geological Engineering faculty and staff. Here, not only I learnt to be a future engineer, but I also learnt to be a better person.

Besides, I would like to express my gratitude to my friends. I am truly grateful for all the friendships and supports I had during my time in OU. Lastly, I would like to say thank you to my family back home, for always trusting on me. You are and always will be my fuel into the future.

Table of Contents

List of Tables

List of Figures

Abstract

Unconventional energy resources, including coal beds, tight gas sands, and shales, have become an ever-increasing factor in the North American gas supply. In these formations, the basic transport properties of the fluids change as they typically travel through sub 100-nm pores, which falls into the field of nanofluidics. As production from shales became economically feasible, this field gained more interest in petroleum engineering.

The purpose of the current study is to determine the effective gas viscosity of shale based on pore scale simulation. We consider methane (CH_4), the main constituent of natural gas, as the only component of fluid system. We use an acyclic pore model to characterize the pore structure of a shale. The acyclic model represents the effective connectivity of pore space because it can capture drainage behavior from mercury injection measurements. We calculate the effective gas viscosity of the shale at different pore pressures, and present the results with respect to the nominal value, under unconfined conditions. Our analysis indicates that the reported permeability from pressure-driven flow measurement has to be considered an effective value, if nominal values of viscosity and density are used for interpretation. That is, we have to modify viscosity and permeability simultaneously in our reservoir model. The current study has a major impact on reservoir characterization based on standard lab measurements in shales.

Chapter 1: Introduction

1.1. Problem Statement

Production in shale formations has been a significant factor in petroleum industry. In 2015, the monthly Energy Review from U.S. Energy Information Administration (EIA) evaluated the natural gas shale potential to fall between 500 and 700 Tcf. Annual Energy Outlook 2016 from EIA expected the total share of shale gas and tight oil plays to grow as much as 69% in 2040. The success of Barnett shale has further enabled the development of many other potential plays such as Woodford and Marcellus shale (Cipolla et al., 2010).

Different from conventional formations, unconventional resources are organic-rich formations and consist of both the source rock and the reservoir. Hydrocarbons in shale are stored in extremely tiny pore space, typically from 2 nm to 100 nm (Eijkel and Berg, 2005; Sparreboom et al., 2009; Loucks et al., 2009; Chalmer et al., 2012; Kovscek et al., 2013; Milliken et al., 2013), therefore they are intrinsically limited in natural permeability (Cramer, 2008). Nevertheless, hydrocarbon production from shales formations was economically feasible because of developments in hydraulic fracturing.

Whereas petrophysical measurements in shales are uncertain and time-consuming in general, pore-scale modeling becomes an important tool to obtain different transport properties, such as viscosity. Although developments in nanofluidics equip researchers with better understanding of transportation in porous media whose sizes are within the nano- range, the problem is the effective viscosity shale gas is not available directly from

lab measurements and existing models in nanofluidics. Furthermore, different from theoretical conduits in nanofluidic devices, natural occurring porous media have more complicated pore structure and topology as they have been modified by different geological phenomena. Therefore, to practically apply knowledge of nanofluidics to porous media such as shales, we must use appropriate pore models to account for the interconnectivity of the pores system at a particular scale of interested.

1.2. Objectives

The present study adopts acyclic pore models as a means to characterize pore structure in shale formations. To further study the effective viscosity in shale, the main objectives are as follows:

- To review viscosity models for gas flow inside a single conduit to determine its value which is relevant to shale formations.
- To calculate the effective viscosity of a shale formation whose pore space is represented by the acyclic pore model.
- To interpret the presented results can help us in order to build a more realistic model based on standard lab measurements.

1.3. Hypothesis

I hypothesize that the effective viscosity is close to the nominal value if we account for the pore structure and pore connectivity in shale formation. To test these hypotheses, we will compare the predicted effective viscosity based on the acyclic pore model with the nominal value.

The acyclic pore model accounts for the effective connectivity of the porous space in shale formation. The model is representative of the pore structure at the core scale as it can capture its permeability and drainage behavior of mercury injection capillary pressure measurement.

Chapter 2: Literature Review

2.1. Nanofluidics

Nanofluidics refers to the study of fluid flow behavior in channels of nanofluidic devices whose characteristic sizes lie within the sub 100-nm range. Therefore, this field is also relevant to hydrocarbon transport in the matrix of shale formation because of its characteristic pore-throat size (Javadpour et al., 2007). The fluid behavior in nano-scale media differs significantly from macroscale ones, therefore advanced knowledge in nanofluidics is crucial to produce economically from unconventional formations (Singh and Singh, 2011).

In nano-scale system, the distance between molecules is comparable to the local characteristic length of porous media at which the relevant fluids' properties are evaluated. Collisions between fluid's molecules are reduced whereas interaction between molecules and the wall increases significantly. Consequently, models of fluid flow based on continuum theory is no longer valid in nano-scale system. When fluids are confined in nano-size conduits, the relevant transport properties, such as viscosity and density, deviate from those reported at ambient conditions.

2.2. Pore scale modeling for rock formations

To study macro-scale behavior in shales, researchers attempted to analyze the transport properties based on different pore-scale models. These models can effectively represent the micro-scale system, and from that, macro-scale behavior can be upscaled accordingly

(Blunt, 2001; Frette et al., 2009; Bandara et al., 2011). Numerous studies in the past allowed us to model the density variation inside a single pore and how hydrocarbon could form an adsorbed layer (Ambrose et al., 2012; Didar and Akkutlu, 2013; Mosher et al., 2013; Jadoon et al., 2016). Recently, Kazemi and Takbiri-Borujeni (2016) accounted for these phenomena by simulating gas displacement inside a single conduit. Although these studies allow us to have a better understanding of mass transport mechanisms in shales, it remains challenged to relate them to the effective transport properties at the core scale.

To bridge the transport properties at the pore scale to those at the large scale, we must build a representative model for the pore space at the core scale. Pore structure modeling is a theoretical approach to analyze pore structure and to capture characteristics of its topology at pore-scale (Bryant et al., 1993; Mousavi and Bryant, 2012). In general, a natural-occurring formation contains of solid grains and the empty space in between, called void spaces. The pore space can further be categorized into 2 different groups based on its characteristic length: pore-throats size and pore-body size. The former refers to the narrowest region of the pore space where different neighboring pores connect, whereas the latter refers to the wider region of the pore.

Among the two types of pore spaces, pore-throats dominate the transport properties of fluids; the smaller pore-throat size leads to fundamental changes in transport properties at the pore scale, such as density and viscosity (Ambrose et al. 2010). Pore-throats also have an impact on the flow conductance, which in turn alters the permeability (Javadour et al. 2007; Sakhaee-Pour and Bryant, 2012; Civan and Devegowda, 2015).

2.2.1. Existing models

In the past, researchers proposed a wide variety of theoretical pore models to capture the effective connectivity of the pore space at the core scale (Washburn, 1921; Fatt, 1956; Mellow, 1989; Sakhaee-Pour and Bryant, 2014; Sakhaee-Pour and Bryant, 2015). These models include the bundle-of-tubes, regular lattice, sphere packing, and acyclic pore model. The core scale is relevant to the size of a typical core, which is usually on the order of few centimeters.

When core measurements are limited, alternative approaches have been derived to calculate different transport properties. Recent studies incorporating production logs have successfully coupled a borehole flow model to determine the relative permeability of a formation (Frooqnia et al., 2011; Frooqnia, 2014). The model allowed us to investigate effective transports properties, which are not possible to measure direct in the lab, at a large scale. Other studies accounted for the pore structure effect to determine the transport properties of a shale (Yu et al., 2015; Ju and Wu, 2016; Ganjdanesh et al., 2016), which can be significantly different from those of highly-permeable formations.

2.2.1.1. Bundle-of-tubes

The first and simplest pore model is the bundle-of-tubes model (Purcell 1949). To relate the mercury injection measurement to permeability, this model simplified the characteristic void spaces in real-scale porous media as various parallel tube sizes, as

shown in **Fig. 1**. The model hypothesized that these parallel tubes can capture the macroscopic transport properties through porous media.

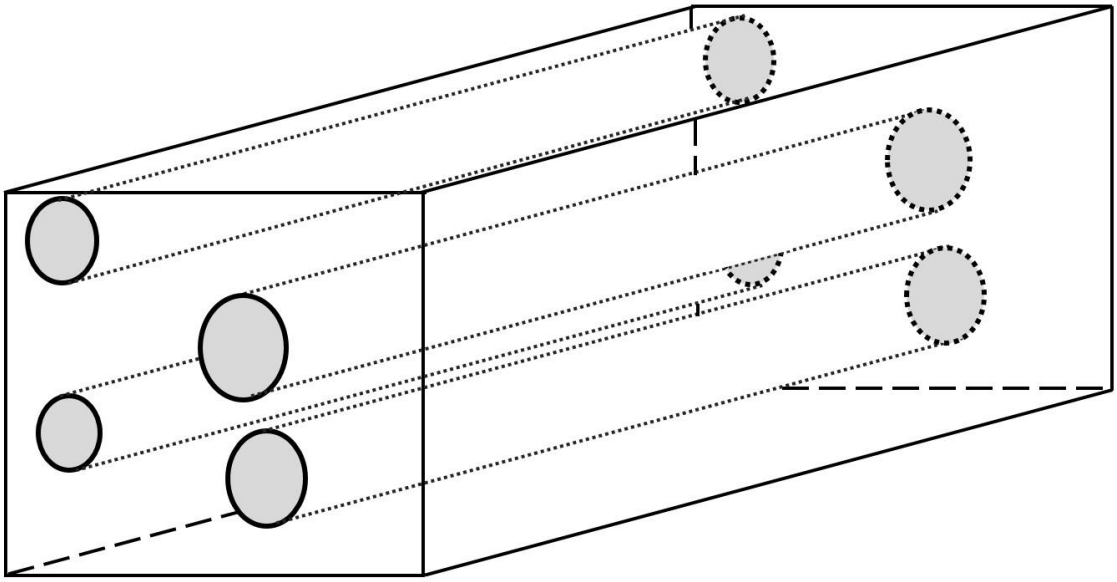

Figure 1— A simple bundle-of-tubes model used to capture the pore structure of rock formation at core scale. The tubes represent the void space and are entailed inside a representative element volume.

At each increasing capillary pressure step, intrusion took place at a characteristic tube size, and Young-Laplace equation governed the relationship between tube sizes and capillary pressure. Although the model could not capture any natural occurring porous media nor the real-scale connectivity of pore space, it pioneered the technique of pore-scale modeling.

2.2.1.2. Regular lattice

To overcome the drawback of bundle of tubes, Fatt (1956) introduced the interconnected tubes model, in which the pore spaces were interconnected in a regular lattice manner (**Fig. 2**). The model has been successfully used to capture the fluid transportation phenomena in conventional rock and ever since a corner stone in modeling. The two-dimensional network of tubes has a random distribution of pore-sizes, and the pore-size distribution can be derived from mercury intrusion measurement.

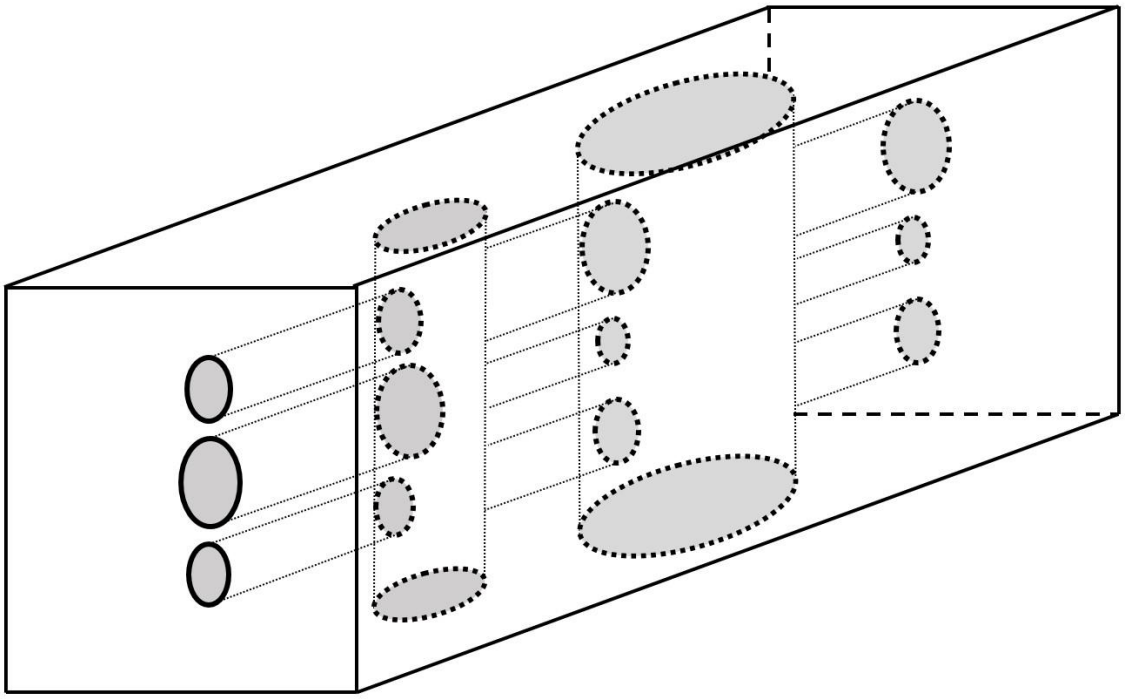

Figure 2— A simple regular-lattice model used to capture pore structure and its effective connectivity at core scale. The tubes represent the pore space, and they are interconnected to each other.

2.2.1.3. Sphere packing

The bundle-of-tubes and regular lattice are fairly simple, yet they fail to represent actual porous media. The major drawback of the model is that it is perfectly anisotropic, whereas the real porous media is usually isotropic (French 2015). To properly represent porous

media, Bryant et al. (1993) proposed a new method to extract a network model from a consolidated granular packing. The sphere-packing model consists of packing of 8000 uniform spheres with known geometry, and assumes that the void-space topology between these spheres physically represent a network model. The position of these spheres has certain impacts on the geometry of the empty space. To create the network model from the void spaces, Bryant et al. (1993) employed Delaunay tessellation (**Fig. 3**); from that, an effective permeability can be calculated and compared to the measured value.

The success of sphere-packing model in unconsolidated sandstones increased interest in using network models to quantify flow properties. Mousavi and Bryant (2007) studied the effect of compaction and cementation on tight-gas sandstone based on the results of the sphere-packing model. The effect of compaction is simulated by considering grains' penetration. Sphere packing proves its effectiveness to study the structure of intergranular void space, which refers to the space between rock grains.

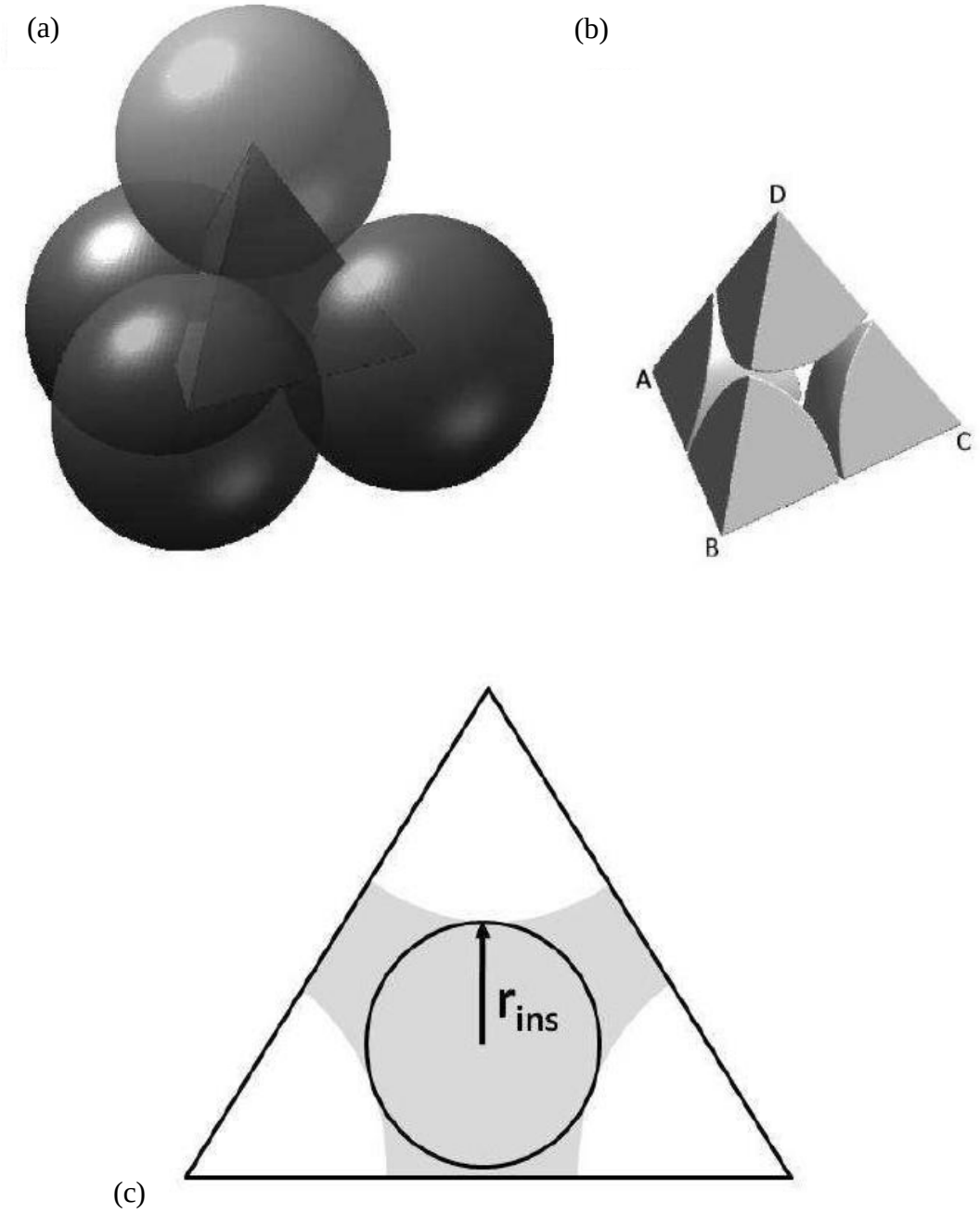

Figure 3—Example of Delaunay tessellation cell, or simple packing of uniform spheres by Mousavi (2010) (a) A tessellation cell with four spherical grains (b) Part of sphere packing inside a smaller pyramid-shaped cell and (c) One face of Delaunay tessellation (throat) with inscribed radius shown by "r_{ins}". The grey area refers to the pore space of the pore-model.

***Courtesy from Mousavi (2010).*

2.2.2. Acyclic pore models

Although sphere packing proves its effectiveness in modeling conventional reservoirs, however, for unconventional formations, the use of this model tends to be inapplicable (Mousavi 2010). In fact, the model only works when we observe a wide range of wetting-phase saturation change corresponding to a small change in relevant capillary pressure (Sakhaee-Pour, 2012). Percolation theory holds true for these conventional formations as long as there exists a plateau-like behavior in drainage curve when capillary pressure (P_c) is plotted against water saturation (S_w) in logarithmic scale (dashed-line in **Fig 4b**).

The situation in unconventional shale formations, however, is rarely the same (Sakhaee-Pour, 2012; Jiang et al., 2015). There is no plateau like trend similar to what has been observed in conventional formations (Fig 4b). It is necessary to analyze fluid flow in shales using a different pore-model. Recently, Sakhaee-Pour (2012) proposed an acyclic model, or tree-like model based on drainage behavior of mercury-injection capillary pressure. In tree-like model, there is a unique path between any two points in the tree-like model (Bethe, 1935) when they are connected (**Fig. 4a**).

The main feature of the tree-like pore model as it relates to our analysis is that the accessibility of wider pore is not restricted by narrower pores; that is, narrower pores are accessible from wider throats. This special feature of tree-like model ensures that no percolation will occur during mercury intrusion. Any change in wetting-phase saturation,

albeit small, will result in an immediate shift in capillary pressure. Additionally, the absence of cycles means that mercury can arrive at any pore provided it reaches the required capillary pressure. The tree-like pore model, therefore, can capture the drainage experiment when the variation of the capillary pressure with wetting-phase saturation exhibits a non-plateau-like trend (straight line **Fig. 4b**).

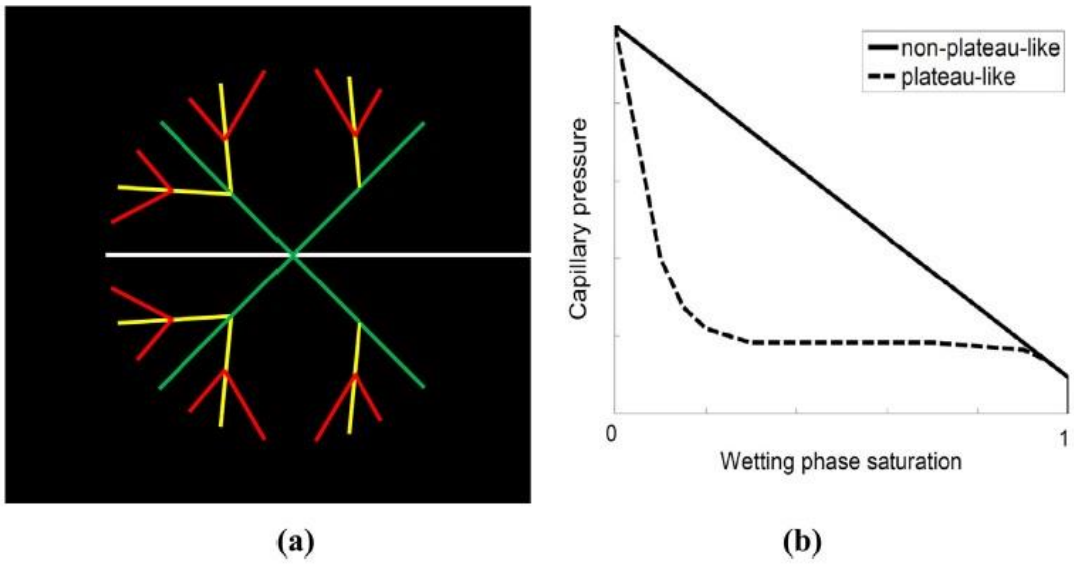

Figure 4—(a) Tree like pore model in which there is a single path between any two points in the model (Bethe, 1935) and narrower pores do not limit the accessibility of wider pores. The red color represents the narrowest conduit and the white color the widest conduit. (b) The tree-like pore model is physically representative of the pore space when a non-plateau-like trend is observed in capillary pressure measurements (Tran and Sakhaee-Pour, 2016).

2.3. Gas viscosity for a single conduit

In this section of the study, we determine how gas viscosity inside a single-nano-size tube deviates from the nominal value at identical pressures and temperatures. We recall that the only component of fluid flow we consider is pure methane. We use the results obtained for single tubes to further calculate the effective viscosity of our current pore-scale model.

2.3.1. Rarefaction effect

We begin our analysis with the definition of the Knudsen number (Kn) to characterize rarefaction effect. Danish physicist Knudsen (1909) defined the dimensionless number Kn as the ratio of the molecular mean-free path to the characteristic length scale, for example, the radius of a pore. Knudsen number allows us to determine the flow regime, from that, we can predict different transport properties using either statistical mechanics or continuum mechanics. Knudsen number can be expressed as follows:

$$Kn = \frac{\mu_{nominal}}{\rho D}\sqrt{\frac{\pi m}{2k_B T}} \tag{1}$$

where Kn is the Knudsen number, $\mu_{nominal}$ is the nominal gas viscosity under unconfined conditions (outside of a conduit), ρ is the gas density, D is the conduit diameter, m is the gas molecular mass, k_B is the Boltzmann constant, and T is the thermodynamics temperature.

2.3.2. Gas viscosity models

In the past, researchers have proposed different models to predict gas viscosity inside a nano-size tube. We normalize the effective viscosity to its nominal value and present the results as a function of the Knudsen number (Kn) as follows:

$$\frac{\mu_{tube}}{\mu_{nominal}} = C(Kn) \tag{2}$$

where μ_{tube} is the gas viscosity inside the conduit, $\mu_{nominal}$ is the nominal viscosity of the gas at identical pressures and temperatures outside of the conduit, and $C(Kn)$ is the rarefaction coefficient defined for a single conduit. **Table 1** lists various models for the rarefaction coefficient available in the literature.

Table 1—Existing models for the rarefaction coefficient, $C(Kn)$, which allows us to relate the gas viscosity inside a single conduit to the nominal value.

Model	$C(Kn)$	Fitting parameters	Range	Reference
1	$\frac{1.3056\,Kn^2+2\pi Kn}{1.3056Kn^2+7.5939Kn+\pi} \times \left(\frac{1}{2}+\alpha_m Kn\right)$	$\alpha_m = \beta_0 + \beta_1 \tan^{-1}\left(\beta_2 Kn^{\beta_3}\right)$ $\beta_0 = 1.2977$ $\beta_1 = 0.71851$ $\beta_2 = -1.17488$ $\beta_3 = 0.58642$	$0 < Kn < 12$	Cercignani (1969)
2	$\frac{1.270042\pi}{2(1+2.222Kn)} \times \left(\frac{1}{2}+\alpha_m Kn\right)$	$\alpha_m = \beta_0 + \beta_1 \tan^{-1}\left(\beta_2 Kn^{\beta_3}\right)$	$0 < Kn < 12$	Sone et al. (1990)

		$\beta_0 = 1.2977$ $\beta_1 = 0.71851$ $\beta_2 = -1.17488$ $\beta_3 = 0.58642$		
3	$\frac{1}{1 + 2Kn + 0.2Kn^{0.788}e^{-\frac{Kn}{10}}}$	-	$0 < Kn < 1$	Veijola and Turowski (2001)
4	$\frac{0.52969Kn + 1.20597}{0.52969Kn^2 + 1.627666Kn + 0.602985985} \times \left(\frac{1}{2} + \alpha_m Kn\right)$	$\alpha_m = \beta_0 + \beta_1 \tan^{-1}\left(\beta_2 Kn^{\beta_3}\right)$ $\beta_0 = 1.2977$ $\beta_1 = 0.71851$ $\beta_2 = -1.17488$ $\beta_3 = 0.58642$	$0 < Kn < 12$	Bahukudumbi et al. (2003)
5	$\frac{1}{1 + 2Kn}$	-	$0.1 < Kn < 10$	Sun and Chan (2003)
6	$\frac{1}{1 + 2.2Kn}$	-	$0.1 < Kn < 10$	Karniadakis et al. (2005)
7	$\frac{1 + 6Kn - 6Kn^2}{1 + 6Kn + 13.5Kn^2}$	-	$0 < Kn < 0.25$	Roohi-NS (2009)
8	$\frac{1 + 0.89Kn + 4.7Kn^2}{1 + 0.75Kn + 19.98Kn^2}$	-	$0.1 < Kn < 0.5$	Roohi-NS (2009)

The ratio of viscosity is related to the rarefaction coefficient by accounting for different parameters which are implemented in the Knudsen number, including the conduit size, gas density, and temperature. It is worth mentioning that the provided models were derived under the assumption that the considered gas has negligible affinity to the pore wall. In other words, these models are applicable to situations where the porous media contains inorganic material.

Unconventional reservoirs, however, such as Barnett shale, usually contain organic matters, therefore it is important to consider the effect of mineralogy if one studies gas transport phenomena in such media (Sakhaee-Pour and Bryant, 2012; Song et al., 2016; Wang et al., 2016). With that in mind, we emphasize that even if the effect of mineralogy is included in our model, our main conclusion, which focuses on the simultaneous modification of viscosity and permeability, does not change.

Next, we shift our focus on the effect of conduit size to the effective viscosity. Results from this analysis will further be used to build a physically representative pore model. We calculate effective viscosity and normalize to its nominal value based on Eq. 2. Different forms of rarefaction coefficients $C(Kn)$ are taken from Table 1. To account for different stages during production of a well, we analyze the results at high and low pressures that are corresponding to the early life of a well and after substantial gas production, respectively.

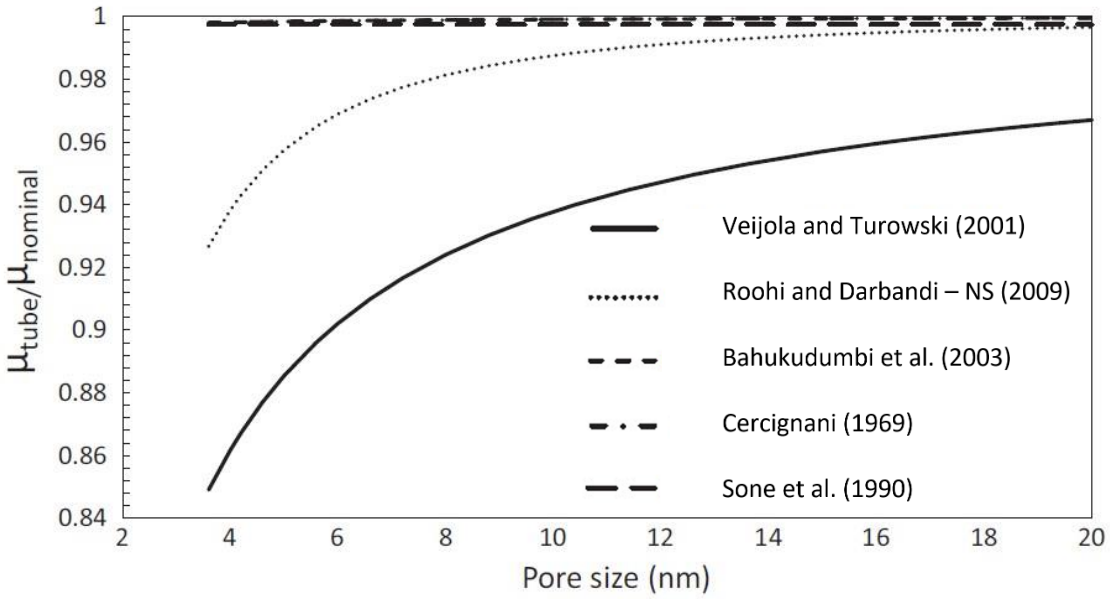

Figure 5— Ratio of the effective gas viscosity to the nominal viscosity inside a single conduit at a high pressure (5000 psia), which is more representative of an early period of production. The deviation from the nominal value increases with decreasing the conduit size, but the difference remains mainly negligible (Tran and Sakhaee-Pour, 2016).

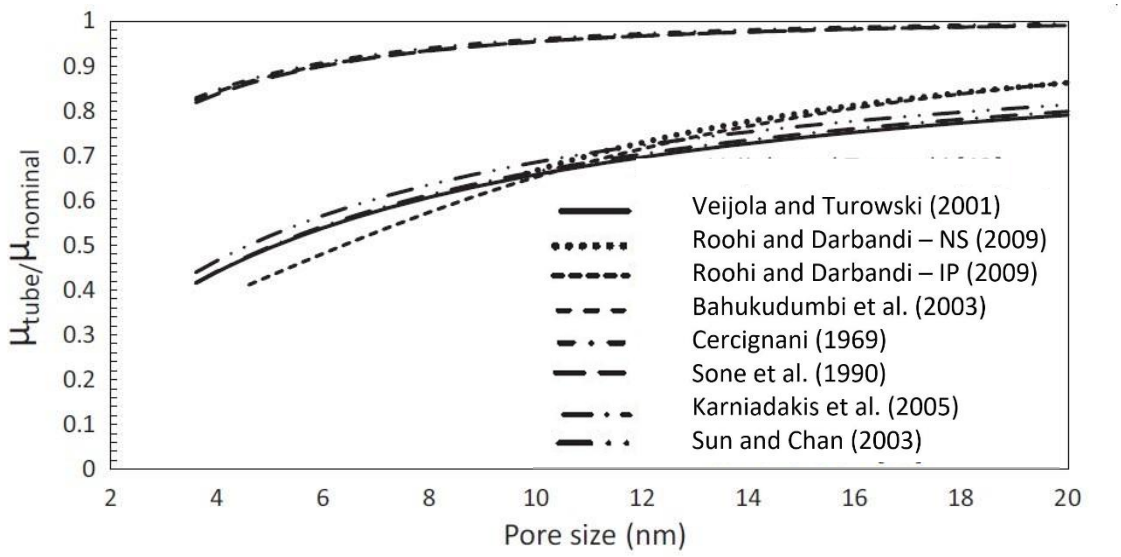

Figure 6— Ratio of the effective gas viscosity to the nominal viscosity inside a single conduit at a low pressure (500 psia), which is more representative of a later period of production. The deviation from the nominal value is significant and increases with decreasing pore-throat size (Tran and Sakhaee-Pour, 2016).

Dependence of the viscosity ratio on conduit sizes for the listed models is illustrated on **Fig. 5** and **6** at 500 and 5000 psi, respectively. The ratio increases and tends to get closer to unity as conduit size becomes larger. The reason behind this trend is that at larger conduit size, or lower Knudsen number (Eq. 1), continuum mechanics governs fluid flow behavior, thus the predicted effective viscosity is closed to its nominal value. The ratio of the viscosity increases from 0.86 to 0.99 at 5000 psi when the conduit size varies between 3.6 and 20 nm, which is typical for a shale. We conclude that at early stage in production, there is no significant deviation from the unconfined value of gas viscosity, regardless of the pore-throat size. More importantly, Fig. 5b further illustrates that the ratio declines to 0.4 when pressure decreases down to 500 psi at later stage of production. The deviation of viscosity from its nominal value is therefore intensified during a later period of production.

Another aspect implemented in our pore-scale model is fluid pressure. We turn our attention to the dependence of viscosity ratio on the effect of fluid pressure within a single conduit. **Figs. 7** and **8** exhibit the change in the ratio within 2-nm and 20-nm conduits, respectively, when pressure increases from 500 to 5000 psi.

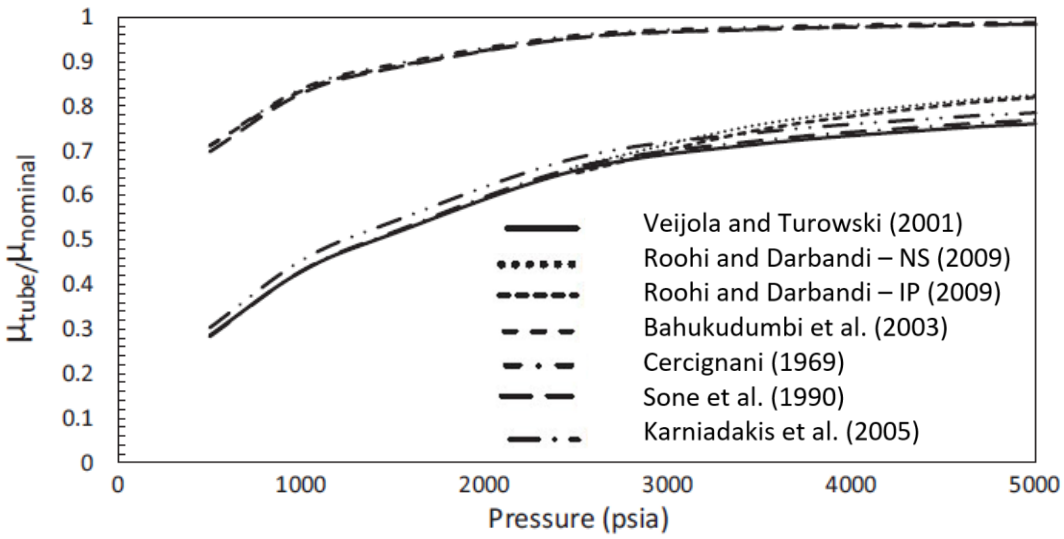

Figure 7— Ratio of the effective gas viscosity inside a 2-nm conduit at different pressures. The deviation from the nominal values is significant even at relatively high pressures based on some models (Tran and Sakhaee-Pour, 2016).

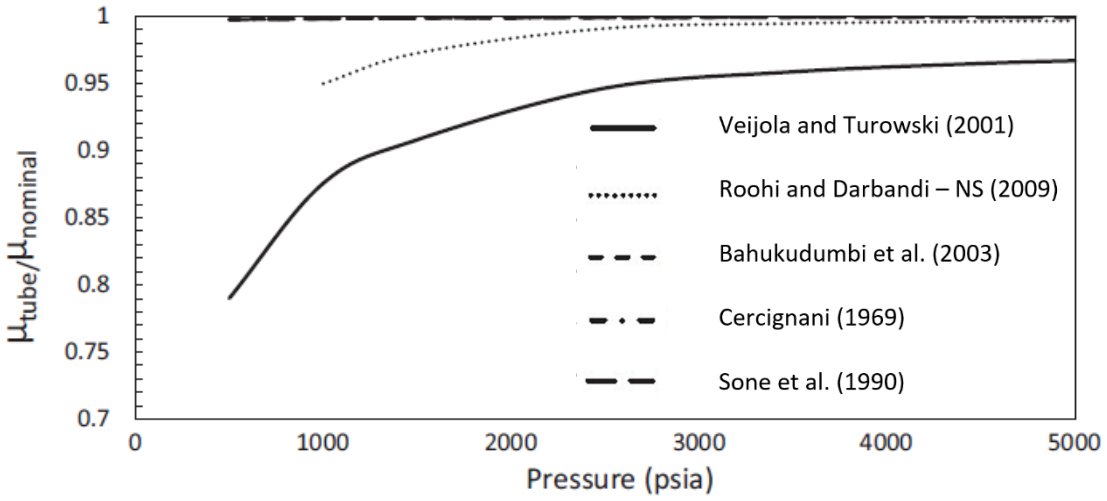

Figure 8— Ratio of the effective gas viscosity inside a 20-nm conduit at different pressures. The deviation from the nominal value remains relatively negligible unless pressure drop below 1000 psi (Tran and Sakhaee-Pour, 2016).

Results indicate that the ratio becomes closer to unity at high pressure. This is because of the dependency of Knudsen number on the pressure, that mitigates the effect of the small conduit size (Eq. 1). Effective viscosity in 20-nm conduit is less close to its nominal value compared to the case in 2-nm. For narrower conduit, the deviation of viscosity remains significant even at relatively high pressure: for instance, the ratio reduces to 0.5 at 2000 psi for some models.

Chapter 3: Methodology

3.1. Pressure driven flow

Our analysis is derived for a pressure-driven flow system, as opposed to shear-driven flow such as Couette flow, simply because it is more relevant to transport in petroleum engineering. In genuine Couette flow, one surface moves tangentially relative to the other surface. This induces a viscous drag force that acts on the fluid in the space between the surfaces, which results in fluid motion. In pressure-driven flow, a pressure gradient is introduced to the system, and fluid motion is in the direction of higher pressure to lower pressure areas.

We first elaborate the effective permeability calculation for the tree-like pore model because it is closely coupled with the effective viscosity in a pressure-driven flow. For this reason, we suppose that the fluid flow takes place from a porous medium, which is at a higher pressure relative to outside.

3.2. Pore-scale model

In the present study, we use the tree-like pore model to characterize the pore space in shale. First, we determine the corresponding permeability of each conduit size to characterize flow conductance. For creeping flow of gas through porous media under no-slip assumption, Hagen-Poiseuille equation governs permeability as follows

$$k_{tube} = \frac{\phi D^2}{32} \tag{3}$$

where k_{tube} is the permeability of the porous medium that includes conduits with similar sizes, D is the corresponding conduit size, and ϕ is the porosity of the sample. We do not account for the effect of tortuosity in the calculation of permeability within single conduits. This is simply because our object is not to analyze the effect of pore-scale model to transport properties in details. In other words, tortuosity factor will not change our conclusion at the end.

We can also compute the total cross-sectional area of the conduits whose characteristic sizes are equal. These conduits are invaded at an equal capillary pressure during drainage. The total cross-sectional area is a strong function of the incremental pore volume invaded at each capillary pressure, which we can determine as follows:

$$A_i L_i = V_p \Delta S_{wi} \tag{4}$$

where A_i is the total cross-sectional area of the conduits invaded at the capillary pressure increment i, L_i is the corresponding total length of the conduits invaded at the corresponding capillary pressure, ΔS_{wi} is the corresponding change in the wetting phase saturation at that capillary pressure, and V_p is the pore volume of the rock.

For simplicity, we take the length of the widest throat to be equal to the length of the sample and we assume the ratio of the lengths of the conduits at sequential pressure is a constant value. Sakhaee-Pour (2012) first defined this ratio as branching ratio. Values of branching ratio in reality are not easy to obtain; in fact, an acyclic model can contain different values of branching ratio for different branches. For the current study, variation of branching ratio redundantly adds to the complexities of the current pore model, and it

does not affect the main conclusion. Therefore, similar to tortuosity, for simplicity, we simply assume that the branching ratio is a constant number in our model.

3.3. Effective viscosity of a pore-scale model

Fig. 9a demonstrates the fluid flow path generated by the tree-like model. The line thickness represents the corresponding pore-throat size. Volume fraction and pore-throat sizes thickness are obtained from mercury intrusion capillary pressure, which will be discussed later. Within the tree-like model, fluid flow takes place from narrower to wider pores. The pressure distribution diagram for the flow patterns is simplified in **Fig. 9b**.

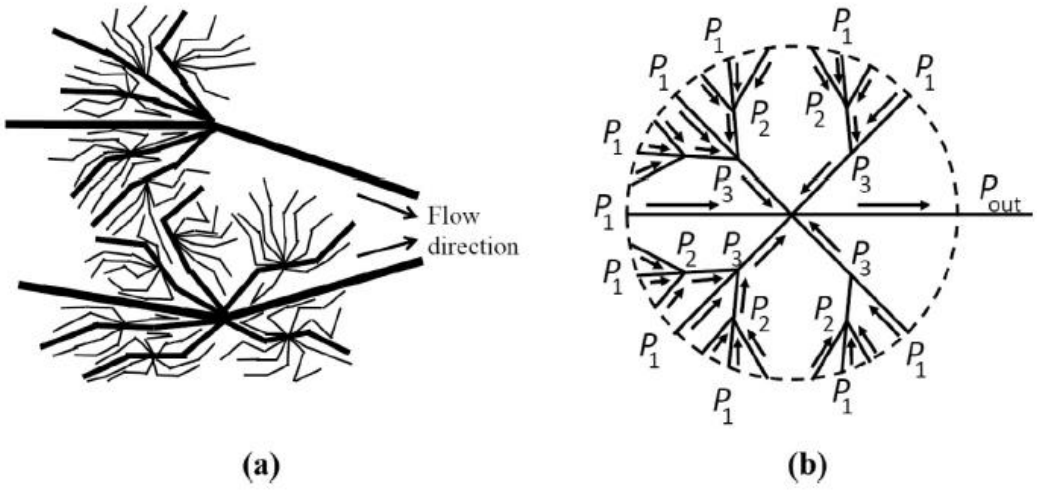

Figure 9—(a) Schematic of flow patterns from the porous medium, whose pore pressure is higher than the outside pressure. (b) Pressure distribution diagram for the flow pattern (Tran and Sakhaee-Pour, 2016).

In pressure-driven flow, fluid displacement takes places from a location with higher pressure to a location with lower pressure in each branch ($P_1 \rightarrow P_2$, $P_2 \rightarrow P_3$, and $P_3 \rightarrow P_{out}$ as in Fig. 7b). This flow assumption allows us to determine the permeability of each

single conduit (Eq. 3). From that, we can also determine the effective permeability of each branch. We are also able to determine the effective permeability of each branch because the pore model is the combination of conduits that act in parallel and in series. The narrowest conduit acts in parallel with a portion of the wider conduit that connects identical pressure (P_1 and P_2 in Fig. 9b). Their outcome acts in series with the remainder of the wider conduit that connects P_2 to P_3. This spatial distribution allows us to derive the effective permeability for the two narrowest conduits as follows:

$$\left(k_{e\_p}\right)_{1\to2}\left(A_{e\_p}\right)_{1\to2} = k_1A_1 + k_2A_2 \tag{5}$$

where $\left(k_{e\_p}\right)_{1\to2}$ is the effective permeability of the pore-scale model between P_1 and P_2 containing the two narrowest conduits and $\left(A_{e\_p}\right)_{1\to2}$ is the corresponding effective area. We use subscript p when the derived parameter is for media that act in parallel and s when they act in series. k_1 is the corresponding permeability of the smallest pore-throat size (Eq. 3) and A_1 is the corresponding total cross-sectional area (Eq. 4). k_1 and A_2 are relevant to the second smallest pore-throat size.

The effective medium, whose permeability is calculated in Eq. 5, acts in series with the remainder of the wider conduits stretched between P_2 and P_3. Thus, we can determine the effective permeability and the cross-sectional area of the two narrowest sizes as follows:

$$\frac{L_{1\to3}}{(k_{e-s})_{1\to3}\,(A_{e-s})_{1\to3}} = \frac{L_{1\to2}}{\left(k_{e-p}\right)_{1\to2}\left(A_{e-p}\right)_{1\to2}} + \frac{L_{2\to3}}{k_2A_2} \tag{6}$$

where $L_{1\to3}$ is the length of Conduit 2 between P_1 and P_3, $L_{1\to2}$ is the length of Conduit 1 between P_1 and P_2, and $L_{2\to3}$ is the length of Conduit 2 between P_2 and P_3 ($L_{1\to3}$ =

$L_{1\to2} + L_{2\to3}$). The pore-throat size of a conduit increases with its number; that is, Conduit 1 is the narrowest conduit and Conduit 2 is the second narrowest conduit in the acyclic model. We denote the effective permeability of the pore-scale model that contains Conduits 1 and 2 between P_1 and P_3 by $(k_{e-s})_{1\to3}$ and its corresponding cross-sectional area by $(A_{e-s})_{1\to3}$.

We repeat this process to find the effective permeability of the pore-scale model. This is an iterative process in which the effective permeability of parallel and series combinations is used for each other. The effective permeability can be calculated as follows:

$$\left(k_{e-p}\right)_{1\to j}\left(A_{e-p}\right)_{1\to j} = (k_{e-s})_{1\to j}\,(A_{e-s})_{1\to j} + k_j A_j \qquad j = 3 \text{ to } n \tag{7}$$

$$\frac{L_{1\to j}}{(k_{e-s})_{1\to j}(A_{e-s})_{1\to j}} = \frac{L_{1\to j-1}}{\left(k_{e-p}\right)_{1\to j-1}\left(A_{e-p}\right)_{1\to j-1}} + \frac{L_{j-1\to j}}{k_{j-1}A_{j-1}} \quad j = 4 \text{ to } n \tag{8}$$

where n is the number of pore-throat sizes, which is equal to the number of capillary pressure measurements. The number of capillary pressure measurements, which is equal to 17 in our study, is usually on the order of 10-100 (Peters, 2012). $\left(k_{e-p}\right)_{1\to j}$ is the effective permeability of the pore-scale model between P_1 and P_j and $\left(A_{e-p}\right)_{1\to j}$ is the corresponding effective area, $(k_{e-s})_{1\to j}$ is the effective permeability of the pore-scale model that contains Conduit 1 and Conduit $(j-1)$ between P_1 and P_j and $(A_{e-s})_{1\to j}$ is the corresponding effective area. $L_{1\to j}$ is the closest distance between P_1 and P_j, $L_{1\to j-1}$ is the closest distance between P_1 and P_{j-1}, and $L_{j-1\to j}$ is the closest distance between

P_{j-1} and P_j in the model. The permeability values calculated here are nominal and relevant to no-slip boundary conditions. We find the nominal permeability of the pore-scale model when j becomes equal to n.

Now, we lump the effect of permeability into effective viscosity calculation. The process is technically a weighted average of the gas viscosity between conduits with different sizes inside the pore-scale model. Similar to the effective permeability calculation, fluid flow takes place from the region with higher pressure to the region with lower pressure. The gas viscosity is dependent on the Kn (Eq. 2), in contrast to the nominal permeability calculation. Thus, we can no longer discard the viscosity terms from the mass balance equation of the pore-scale model. We did not account for the shale gas compressibility, which is different from the value used in conventional reservoirs with large pores. The compressibility value depends on the pore size in a shale formation because the pore pressure does not change significantly at the pore scale in a single-phase flow. Furthermore, this observation also allows to use a constant value of pore pressure across different conduits of the pore model

Considering that the narrowest conduits act in parallel with part of the wider conduit that connect identical pressure (P_1 and P_2), we can calculate the effective viscosity as follows:

$$\frac{1}{\left(\mu_{e-p}\right)_{1\to2}} = \frac{1}{\left(k_{e-p}\right)_{1\to2}\left(A_{e-p}\right)_{1\to2}}\left(\frac{k_1A_1}{\mu_{tube-1}} + \frac{k_2A_2}{\mu_{tube-2}}\right) \tag{9}$$

where $\left(\mu_{e-p}\right)_{1\to2}$ is the effective viscosity of fluid flow inside Conduits 1 and 2, μ_{tube-1} is the gas viscosity inside Conduit 1, and μ_{tube-2} is the gas viscosity inside Conduit 2.

We can express the ratio of the effective viscosity to the nominal value to define the effective rarefaction coefficient as follows:

$$\left(C_{e-p}\right)_{1\to2} = \frac{\left(\mu_{e-p}\right)_{1\to2}}{\mu_{nominal}} = \frac{\left(\mathrm{k}_{e-p}\right)_{1\to2}\left(\mathrm{A}_{e-p}\right)_{1\to2}}{\frac{k_1A_1}{C_1(Kn)} + \frac{k_2A_2}{C_2(Kn)}} \tag{10}$$

where $\left(C_{e-p}\right)_{1\to2}$ is the effective rarefaction coefficient for the gas phase between P_1 and P_2 through Conduits 1 and 2, and C_1 and C_2 are the corresponding rarefaction coefficients.

The effective medium acts in series with the remainder of the wider conduits stretched between P_2 and P_3. Thus, we can determine the effective rarefaction coefficient as follows:

$$\begin{aligned}(C_{e-s})_{1\to3} &= \frac{(\mu_{e-s})_{i\to3}}{\mu_{nominal}} \\ &= \frac{(\mathrm{k}_{e-s})_{1\to3}(A_{e-s})_{1\to3}}{L_{1\to3}} \left(\frac{\left(C_{e-p}\right)_{1\to2}L_{1\to2}}{\left(\mathrm{k}_{e-p}\right)_{1\to2}\left(A_{e-p}\right)_{1\to2}} + \frac{C_2L_{2\to3}}{k_2A_2}\right)\end{aligned} \tag{11}$$

where $(C_{e-s})_{1\to3}$ is the effective rarefaction coefficient for gas flow between P_1 and P_3 through Conduits 1 and 2 whose effective viscosity is represented by $(\mu_{e-s})_{1\to3}$.

The calculation of the effective rarefaction coefficient of the pore-scale model is an iterative process similar to the effective permeability calculation. We repeat the calculation of the effective rarefaction coefficients of the media that act in series and in parallel to determine the effective viscosity of the pore-scale model as follows:

$$\left(C_{e-p}\right)_{1\to j}=\frac{\left(\mu_{e-p}\right)_{1\to j}}{\mu_{nominal}}=\frac{\left(k_{e-p}\right)_{1\to j}\left(A_{e-p}\right)_{1\to j}}{\frac{(\mathrm{k}_{e-s})_{1\to j-1}(\mathrm{A}_{e-s})_{1\to j-1}}{(C_{e-s})_{1\to j-1}}+\frac{k_{j-1}A_{j-1}}{C_{j-1}}}\quad j=3\text{ to }n \tag{12}$$

$$\begin{aligned}(C_{e-s})_{1\to j}&=\frac{(\mu_{e-s})_{1\to j}}{\mu_{nominal}}\\&=\frac{(k_{e-s})_{1\to j}(A_{e-s})_{1\to j}}{L_{1\to j}}\left(\frac{\left(C_{e-p}\right)_{1\to j}L_{1\to j-1}}{\left(k_{e-p}\right)_{1\to j-1}\left(A_{e-p}\right)_{1\to j-1}}\right.\\&\left.+\frac{C_{j-1}L_{j-1\to j}}{k_{j-1}A_{j-1}}\right)\qquad j=4\text{ to }n\end{aligned} \tag{13}$$

where $\left(C_{e-p}\right)_{1\to j}$ and $(C_{e-s})_{1\to j}$ are the effective rarefaction of the media when they act in parallel and in series, respectively, and n is the number of conduit sizes used. The effective rarefaction of the pore-scale model is equal to $(C_{e-s})_{1\to j}$ when j becomes equal to the number of pore-throat sizes (n).

Chapter 4: Results and Discussion

4.1. Mercury injection capillary pressure

In this section, we characterize the pore-space of a shale at the core scale based on drainage result from mercury intrusion test. Drainage test is representative of the connected pore-throat size at the core scale. An alternative approach to directly capture the pore-space system is to analyze high-resolution images and then extract the pore model. However, it is not possible yet to obtain a pore model that can be representative of the core scales from such images alone. Furthermore, such approach does not account for the effect of confinement. In other words, the pore-space system obtained from the high-resolution images is not representative of the in-situ conditions. Some opened fractures observed from high-resolution images might be closed at subsurface conditions.

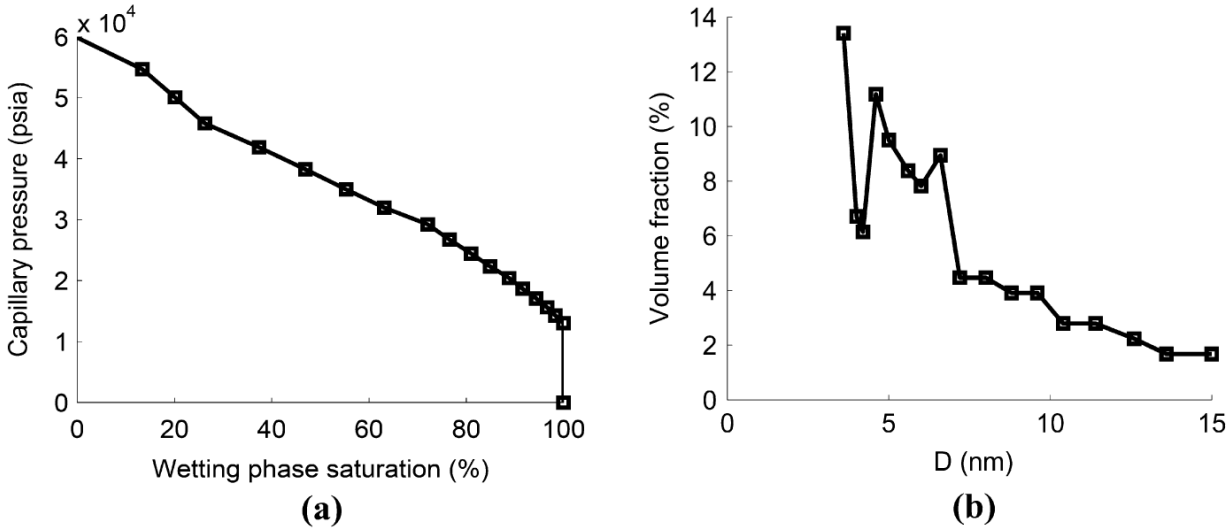

Figure 10—(a) Capillary pressure measurements (Dewers et al., 2012) of a shale sample that is used for effective viscosity calculation. Drainage behavior exhibits a non-plateau-like trend, which indicates that the tree-like model can be used to capture the connectivity of the pore structure at the core scale (Sakhaee-Pour and Bryant, 2015). (b) Pore-throat size distribution of the sample derived from the

Fig. 10a and **b** illustrate the drainage test from a shale sample and its pore-throat size distribution under confinement, respectively. During drainage test, volume fraction of mercury (S_{Hg}), which is a non-wetting phase, increases at higher capillary pressure. From that, the wetting phase fraction, which is usually water (S_w), can be deducted as $S_w = 1 - S_{Hg}$, during the test. Fig. 8a further shows that the intrusion actually occurs when capillary pressure increases up to 15,000 psi. More important, the shale exhibit a non-plateau-like trend in capillary pressure increment. That is, the capillary increases linearly with decreasing non-wetting phase saturation. Sakhaee-Pour and Bryant (2015) proved that when such non-plateau-like increase occurs during mercury intrusion in a shale, the tree-like pore model can be used to depict the connectivity of pore-space inside the porous medium.

Drainage test conducted on the shale core plug allows us to derive its pore-throat size distribution for our study (Fig 10b). The pore-throat sizes distribution is representative of the effective connectivity at the core scale because it accounts for the effect of confinement on the pore-space. The measurements were conducted under confined boundary conditions, which close microfractures, at least partially.

As showed previously from Fig. 5 and 6, the deviation of effective gas viscosity from its nominal value becomes important when conduit size decreases. In our study, the largest pore-throat size is on the order of 15 nm (Fig. 10b), which implies that the void space corresponds to the matrix of a formation. The average pore-throat size increases when

there are open micro fractures. Hence, our analysis is relevant to the condition where the deviation from a nominal value is more significant, by including ultra-narrow throats.

4.2. Results

Now, we calculate the effective gas viscosity of the shale sample from our proposed tree-like pore model. The methodology has been described in details in Chapter 3, section 3.2 and 3.3. The effective gas viscosity is dependent on several factors. First, we analyze the effect of branching ratio on the effective gas viscosity at high and low pressure. It is worth emphasizing that for simplicity, we assume that branching ratio is a constant throughout the entire pore-model. We present the results using the two models from Veijola and Turowski (2001) and Bahukudumbi et al. (2003) that cap the upper and lower bounds based on our analysis for the gas viscosity of single conduit, respectively. **Fig. 11** shows the effect of branching ratio on the effective gas viscosity.

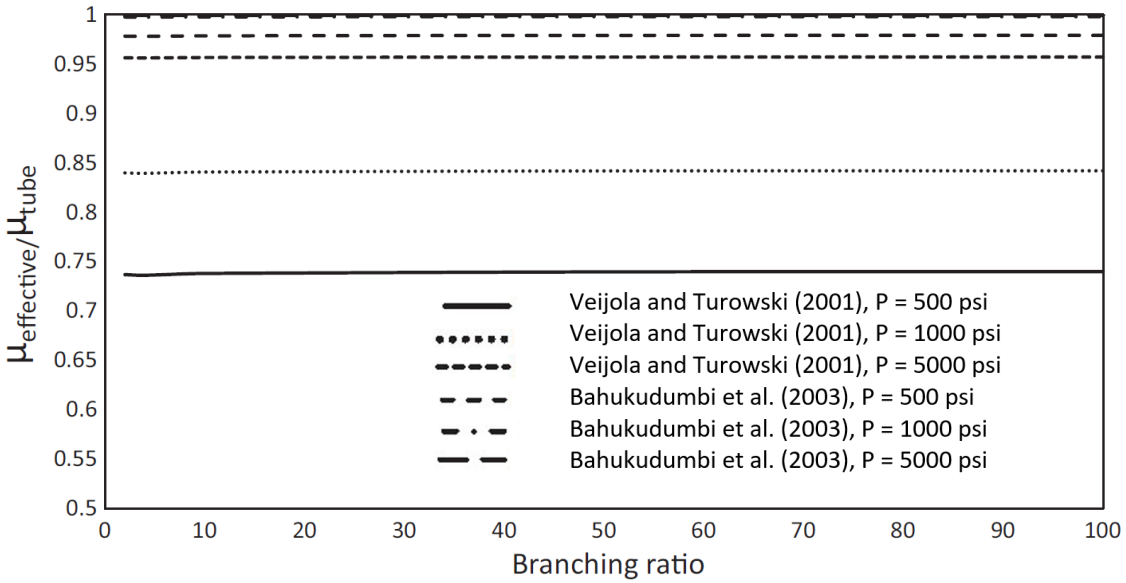

Figure 11— Effect of the branching ratio on the ratio of the effective viscosity to the nominal viscosity is negligible. We use only the two models that provide upper and lower bounds for the effective viscosity (Tran and Sakhaee-Pour, 2012).

Effective viscosity ratio turns out to be independent on the branching ratio. We recall that branching ratio represents the length ratio of conduits of the model at sequential pressures. Although the branching ratio has significant impact on the topology of the pore-scale model, results from Fig. 9 indicates that it has negligible influence on the effective gas viscosity.

Next, we analyze the dependency of the effective viscosity on the pore pressure. Because the effect of branching ratio on effective viscosity is negligible (Fig. 11), we only select two branching ratios to demonstrate the change in effective gas viscosity as a function of pore pressures (**Fig. 12**).

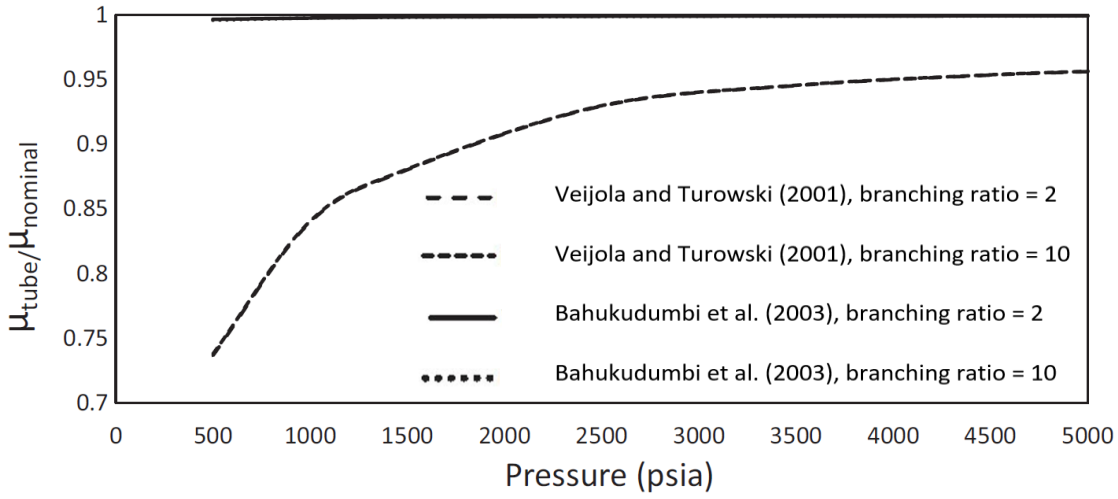

Figure 12— Ratio of the effective viscosity to the nominal viscosity as a function of pore pressures with two branching ratios for the two models that provide the upper and lower bounds for the effective viscosity (Tran and Sakhaee-Pour, 2012).

For a typical pore-throat size relevant to a shale formation (Fig. 10b), the Knudsen number (Kn) is on the order of 0.15 - 0.64 when the pore pressure is 500 psi, and it varies between 0.02 and 0.08 when the pressure becomes equal to 5000 psi. The ratio of the effective viscosity to the nominal viscosity remains larger than or equal to 0.9 when the pore pressure is larger than or equal to 2000 psi. The ratio decreases with decreasing pore pressure but remains larger than 0.75 when the pore pressure varies between 2000 and 500 psi. Thus, the difference between the effective viscosity and the nominal viscosity is negligible at an early period of production. The deviation from the nominal value is relatively important only at a late period of production because of the increase in the Kn, mainly due to a decline in density.

Another important observation from Fig. 12 is that the smallest ratio is close to 0.73 based on the acyclic pore model. From Fig. 6a and b, it can be seen that this ratio lays between

the smallest ratio corresponding to a 20-nm conduit (0.78) and a 2-nm conduit (0.28). Although the effective viscosity takes connectivity of different pore-sizes into account, the current result implies that the effective viscosity is primarily controlled by wider conduits. Therefore, we propose that there exists an effective pore-throat size that dominates the effective viscosity. **Fig. 13** demonstrates our calculation of the characteristic pore-throat size.

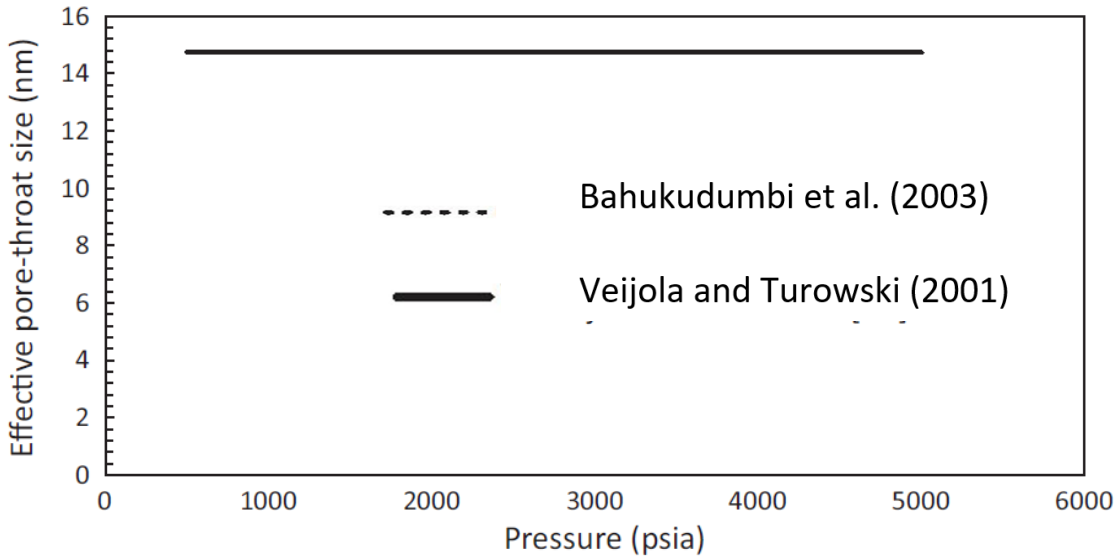

Figure 13— Effective pore-throat size, whose corresponding effective viscosity is equal to the effective viscosity of the pore-scale model, is almost equal to the largest pore-throat size included in the tree-like pore model. The branching ratio is set equal to 2 here for the effective pore-throat size calculation because it plays a negligible role (Tran and Sakhaee-Pour, 2012).

Similarly, we only select the two models that result in the upper and lower bounds for the effective viscosity, Bahukudumbi et al. (2003) and Veijola and Turowski (2001), respectively. Additionally, an arbitrary value of branching ratio is set equal to 2 for the purpose of demonstration only because it has no impact on the prediction of effective gas

viscosity, as illustrated in previous sections. From Fig. 11, we can see that the effective pore-throat size is closer to the largest pore-throat size reported based on drainage result (Fig. 10b). More importantly, the ratio is independent of the pore pressure.

To explain the result, we consider the topology of the current pore-scale model. We recall that in tree-like model, the largest conduit acts in series with the remainder of the pore system. When pore pressure is applied to the pore-scale model, the largest pore-size will possess the smallest value of Knudsen number (Kn). Which, in turn, implies that widest conduit will also has the largest effective gas viscosity, or the effective gas viscosity ratio. The largest viscosity results in a higher resistance against the flow that is important at the pore-scale because it acts in series with remainder of the pore space. This does not necessarily mean that the effective transport properties of the wider pores are inferior in a nanofluidic system because we only analyze the effective viscosity and not the overall transport.

4.3. Validation of the current network modeling approach

In the section of the chapter, we will look at the validation of the current modeling approach. The network modeling approach used in this study has been tested against different lab measurements. First, Sakhaee-Pour and Bryant (2012) used the network modeling approach to predict gas permeability for different pore pressures. They accounted for the combined effects of an adsorbed layer and slippage on the flow conductance of a single conduit. They then related the results to the transport properties

of a core plug by taking into account the interactions among the pores. They tested the results against lab measurements.

Sakhaee-Pour and Bryant (2015) subsequently used the network modeling approach to capture the no-slip permeability of a shale formation based on mercury intrusion capillary pressures, which allowed them to develop the acyclic pore model. The predicted results were compared with reported no-slip permeability. More recently, Sakhaee-Pour and Li (2016) showed that not only the acyclic pore model can capture the capillary pressures measurements of a shale but also can characterize its fractal properties relevant to pore-throat and pore-body sizes.

4.4. Discussion

The dependency of the viscosity of the conduit size is an intrinsic characteristic of a nanofluidic system, which is relevant to shales because their pore-throat sizes are usually smaller than 20 nm. The dependency becomes insignificant in more permeable formations because of their wider pores. There are different sizes associated with each pore, such as pore-throat size and pore-body size. The pore-throat size is more relevant to the flow resistance between neighboring pores, as opposed to the pore-body size; hence, we used the pore-throat size obtained from drainage in our study.

The gas viscosity is predicted based on Knudsen number (Kn), which is proportional to the inverse of the characteristic size (Eq. 1). The viscosity deviation from the nominal value becomes more significant when this dimensionless number increases. Thus, using

pore-throat size, which is the narrowest region of a pore for a given pressure and temperature, allowed us to determine the effect of viscosity change when its deviation from the nominal value is maximum. Based on our analysis, the effect of such deviation on the effective transport properties at the core scale is negligible. The deviation from the effective core-scale properties is even less significant if we use other characteristic sizes of a pore.

To determine the effective viscosity, we presented the results with respect to the nominal permeability. We did not account for the shale gas compressibility, which is different from the value used in conventional reservoirs with large pores. The compressibility value depends on the pore size in a shale formation because the pore pressure does not change significantly at the core scale in a single-phase flow. The determined viscosity remains an effective transport property, similar to the permeability, if it is based on the interpretation of lab measurements with nominal values. The interpretation of lab measurements for effective viscosity was the main objective of our study, which was a thought experiment.

4.4.1. Practical implication

The gas viscosity inside a nano-size conduit is lower than the nominal value. The lower viscosity enhances the flow rate, whose effect is similar to that of gas slippage. We were able to differentiate the viscosity effect because the viscosity models in the literature are reported for a shear- driven flow, as opposed to a pressure drive flow. It is impossible to

distinguish the viscosity and the slippage effects based on pressure driven measurements based on the nature of Hagen-Poiseuille or Darcy's equation.

Thus, the permeability values reported based on lab measurements also embrace the viscosity effect and should be considered effective transport properties, rather than permeability values, when we use nominal values for viscosity and density. The practical implications of this are that we should not implement viscosity and permeability values separately in reservoir models if the permeability value is based on lab measurements with nominal parameters.

4.4.2. Limitations

Although the present work discusses the fundamental transport properties of shale, there are certain drawbacks that we should consider. First, the model only analyzes flow of single-phase fluid. More importantly, the single-phase fluid is assumed to be pure methane. While these assumptions simplify the process, it is not realistic to have any porous media consisting of a pure gas. Furthermore, different gases have different interactions with the pore wall. Consequently, this leads to a change of *Kn* within a single conduit, thus affecting the whole pore-scale model as a whole.

The provided models to calculate effective viscosity are based on the assumption that the gas has a minimum affinity to the pore wall. Therefore, the study is limited to the case of inorganic material.

Mechanics of fluid flow follows the study of nanofluidics in the current study. Therefore, models based on continuum mechanics, such as Hagen-Poiseuille or Darcy's equation, is invalid. However, when effective viscosity is analyzed for many nano-size conduits within the acyclic model, we still utilize the conventional mass balance equation to derive the results.

4.4.3. Future work

In order to build a more realistic pore-model, we can introduce different components into the fluid flow system. Furthermore, we can consider the case when gas flow takes place inside an inorganic material. When gas flow takes place inside an organic material, similar to Barnett shale, the effect of a minerology has to be implemented for gas transport.

Conclusions

Nanofluidics, which analyzes fluid transport through sub 100-nm conduits, recently gained significant interest in petroleum engineering, as the characteristic pore-throat size of shale formation is usually smaller than 20 nm. The effect of gas rarefaction takes place in nano-size conduits as the gas mean-free path is on the same order of magnitude with the characteristic length of the conduits. This results in a deviation of the basic transport properties inside nano-size conduits from the nominal values reported without the effect of confinement.

With this in mind, we first determined the ratio of the effective viscosity to the nominal viscosity inside a circular conduit for methane (CH_4) using different models. In general, the viscosity ratio is expressed in terms of Knudsen number (Kn). Our study for a single conduit shows the effective viscosity remains close to the nominal value at high pressure (~5000 psi), regardless of the pore-throat size. At low pressure (~500 psi), the ratio of the effective viscosity to the nominal value decreases to 0.2 – 0.7, based on different models.

We then adopted the tree-like pore model to account for the effective connectivity of the pore space at the core scale. The tree-like pore model interconnects the conduits in a manner similar to a tree's branches. The most important features of the pore-scale model are that there is a single path between any two points in the pore-scale model and narrower pores are accessible only from a wider pore. More importantly, the model is able to capture the non-plauteau-like behavior of capillary pressure measurements obtained from mercury intrusion in shale. Therefore, it successfully accounts for the effective connectivity of the pore space of shale at the core scale.

Our pore-scale model reveals that the effective viscosity of the pore-scale model is close to the corresponding value of the largest pore-throat size based on pore-throat size distribution. The deviation of the effective pore-throat size is negligible over a wide range of pore pressure. This is mainly because of the topology of the tree-like pore model, where the widest pore acts in series with the remainder of the pore space, and plays a crucial role in controlling the transport properties.

The gas viscosity inside a nano-size conduit is smaller than the nominal value, which improves the flow rate in a manner similar to gas slippage. We were able to differentiate these effects because the viscosity models were based on shear-driven flow while the slippage is often account for in pressure-driven flow. It seems impossible to differentiate the effects of viscosity and slippage if we only analyze the pressure-driven flow, which is used for permeability measurements.

Thus, the reported permeability in a pressure-driven flow has to be considered an effective transport property if nominal viscosity and density are used for interpretation. In other words, we have to modify viscosity and permeability simultaneously in our reservoir model for shale formations. This study has major implications for reservoir characterization based on standard lab measurements for shales.

References

Ambrose, R.J., Hartman R.C., Diaz Campos, M., Akkutlu, I.Y., Sondergeld, C. 2010. New pore-scale considerations for shale gas in place calculations. Paper SPE-131772 presented at the SPE unconventional gas conference, Pennsylvania.

Ambrose, R.J., Hartman, R.C., Diaz-Campos, M., Akkutlu, I.Y., Sondergeld, C. 2012. Shale gas-in-place calculations Part I: new pore-scale considerations. *SPE J* **17**(1): 219–229

Bandara, U.C., Tartakovsky, A.M., and Palmer, B.J. 2011. Pore-scale study of capillary trapping mechanism during CO_2 injection in geological formations. *International Journal of Greenhouse Gas Control* **5**:1566–1577.

Bahukudumbi, P., Park, J.H., and Beskok, A. 2003. A unified engineering model for steady and quasi-steady shear-driven gas microflows. *Microscale Thermophys Eng.*

Bethe, H.A. Statistical theory of superlattices. *Proc R Soc Lond* A **150**(871):552–575.

Blunt, M.J. 2001. Flow in porous media – pore-network models and multiphase flow. *Current Opinion in Colloid and Interface Science* **6**, 197–207.

Bryant, S., Cade, C., and Mellor, D. 1993. Permeability prediction from geologic models. *AAPG Bulletin* **77**(8): 1339–1350.

Cercignani, C. 1969. Mathemathical methods in kinetic theory. 1st ed. US:Springer.

Chalmers, G.R., Bustin, R. M., and Power, I. M. 2012. Characterization of gas shale pore systems by porosimetry, pycnometry, surface area, and field emission scanning electron microscopy/transmission electron microscopy image analyses: Examples from the Barnett, Woodford, Haynesville, Marcellus, and Doig units. *AAPG Bulletin* **96**(6): 1099–1119.

Cipolla, C.L., and Lolon, E.P. 2010. Reservoir Modeling in Shale-Gas Reservoirs. Paper SPE–125530 presented at the SPE Eastern Regional Meeting, Charleston, West Virginia, USA, 23–25 September.

Civan, F., and Devegowda, D. 2015. Comparison of shale permeability to gas determined by pressure-pulse transmission testing of core plugs and crushed samples. Paper SPE-178571 presented at the SPE unconventional resources technology conference, Texas.

Cramer, D.D. 2008. Stimulating Unconventional Reservoirs: Lessons Learned, Successful Practices, Areas for Improvement. Paper SPE–114172–MS presented at the SPE Unconventional Reservoirs Conference held in Keystone, Colorado, USA, 10–12 February.

Dewers, T.A., Heath, J., Ewy, R., Duranti, L. 2012. Three-dimensional pore networks and transport properties of a shale gas formation determined from focused ion beam serial imaging. *Int J Oil, Gas Coal Technol*. **5**(2-3):229―249.

Didar, B.R., and Akkutlu, I.Y. 2013. Pore-size dependence of fluid phase behavior and properties in organic-rich shale reservoirs. Paper SPE-164099 presented at the SPE international symposium on oilfield chemistry, Texas.

Eijkel, J.C.T, and Berg, A.V.D. 2005 Nanofluidics: what is it and what can we expect from it?. *Journal of Microfluidics and Nanofluidics* **1**(3): 249―267.

Fatt, I. The network model of porous media. I. Capillary pressure characteristics. *Pet Trans AIME* **207**:144–181.

French, L.B. 2015. Multiscale Modeling of Particle Transport in Petroleum Reservoirs. Master's Theses, Louisiana State University and Agricultural and Mechanical College, Louisiana, USA.

Frette, O.I., Virnovsky, G., and Hildebrand-Habel, T. 2009. Modeling the stability of thin water film using SEM images. Paper SPE-121250-MS presented at the EUROPEC/EAGE Conference and Exhibition held at Amsterdam, The Netherlands, 8–11 June.

Frooqnia, A., A-Pour, R., Torres-Verdín, C., and Sepehrnoori, K. 2011. Numerical simulation and interpretation of production logging measurements using a new couple wellbore-reservoir model. Paper SPWLA VV. presented at the SPWLA 52nd international logging symposium, Colorado.

Frooqnia, A. Numerical simulation and interpretation of borehole fluid-production measurements. Ph.D. dissertation. The University of Texas at Austin, Austin, Texas.

Ganjdanesh, R., Rezaveisi, M., Pope, G.A., Sepehrnoori, K. 2016. Treatment of condensate and water blocks in hydraulic-fractured shale-gas /condensate reservoirs. *SPE J* **21**(2):665–674

Jadoon, Q.K., Roberts, E., Blenkinsop, T., Wust, R.A., Shah, S.A. 2016. Petrophysical evaluation and uncertainty analysis of Roseneath and Murteree shales reservoirs in Cooper Basin, Australia (a case study). *J Petrol Sci Eng* **146**: 330–345.

Javadpour, F., Fisher, D., and Unsworth, M. 2013. Nanoscale gas flow in shale gas sediments. *J Can Pet Technol* **46**(10).

Jiang, C., Bryant, S., and Daigle, H. 2015. A Bundle of Short Conduits Model of the Pore Structure of Gas Shale. Paper URTEC-2169349-MS presented at the Unconventional Resources Technology Conference held at San Antonio, Texas, USA, 20–22 July.

Ju, B., and Wu, D. 2016. Experimental study on the pore characteristics of shale rocks in Zhanhua depression. *J Petrol Sci Eng* **146**:121–128.

Karniadakis, G.E., Beskok, A., and Aluru, N. 2005. Microflows and Nanoflows. *Interdisciplinary Applied mathematics.* New York: Springer-Verlag.

Kazemi, M., and Takbiri-Borujeni. 2016. Non-equilibrium molecular dynamics simulation of gas flow in organic nanochannels. *J Natural Gas Sci Eng* **33**: 1087–1094.

Knudsen, M. 1909. The laws of molecular and viscous flow of gases through tubes. *Ann Phys* **333**(1):75–130.

Kovscek, A., and Alnoaimi, K. 2013. Experimental and Numerical Analysis of Gas Transport in Shale Including the Role of Sorption. Paper SPE–166375 presented at the SPE Annual Technical Conference and Exhibition held in New Orleans, Louisiana, USA, 30 September–2 November.

Loucks, R.G., Reed, R.M., Ruppel, S.C., Jarvie, D.M. 2009. Morphology, genesis, and distribution of nanometer-scale pores in siliceous mudstones of the Mississippian Barnett Shale. *Journal of sedimentary Research* **79**(12): 848–861.

Mellow, D.W. 1989. Random close packing (RCP) of equal spheres: structure and implications for use as a model porous medium. PhD dissertation. UK: Open Univeristy.

Milliken, K.L., Rudnicki, M., Awwiller, D.N., Zhang, T. 2013. Organic matter-hosted pore system, Marcellus Formation (Devonian), Pennsylvania. *AAPG Bulletin* **97**(2): 177–200.

Mosher, K., He, J., Liu, Y., Rupp, E., Wilcox, J. 2013. Molecular simulation of methane adsorption in micro- and mesoporous carbons with applications to coal and gas shale systems. *Int J Coal Geol* **109**: 36–44.

Mousavi, M.A., and Bryant, S.L. 2012. Connectivity of pore space as a control on two-phase flow properties of tight-gas sandstones. *Transp Porous Media* **94**(2): 537–554.

Mousavi, M.A., and Bryant, S.L. 2007. Geometric Models of Porosity Reduction mechanisms in Tight gas sands. Paper SPE-107963 presented at the SPE Rocky Mountain Oil and Gas Technology Symposium, Denver, Colorado, USA.

Mousavi, M.A. 2010. Pore-scale Characterization and Modeling in Two-phase Flow in Tight Gas Sandstones. PhD dissertation, The university of Texas at Austin, Austin, Texas, USA.

Purcell, W.R. 1949. Capillary pressure-their measurement using mercury and the calculation of permeability therefrom. *J Petrol Technol* **1**(2):39–48.

Roohi, E., and Darbandi, M. 2009. Extending the Navier-Stokes solutions to transition regime in two-dimensional micro- and nanochannel flows using information preservation scheme. *Phys Fluids* **21**(8).

Sakhaee-Pour, A., and Bryant S.L. 2012. Gas permeability of shale. *SPE Reservoir Eval Eng* **15**(4):401–409.

Sakhaee-Pour, A., and Bryant, S.L. 2014. Effect of pore structure on the producibility of tight-gas sandstones. *AAPG Bulletin* **98**(4):663–694.

Sakhaee-Pour, A., and Bryant, S.L. 2015. Pore structure of shale. *Fuel* **143**:467–475.

Singh, S.K., and Singh, J.K. 2011. Effect of pore morphology on vapor-liquid phase transition and crossover behavior of critical properties from 3D to 2D. *Fluid Phase Equilib* **300**(1-2): 182–187.

Sone, Y., Takata, S., and Ohwada, T. 1990. Numerical analysis of the plane Couette flow of a rarefied gas on the basis of the linearized Boltzmann equation for hard-sphere molecules. *Eur J Mech* **9**:273–288.

Song, W., Yao, J., Li, Y., Sun, H., Zhang, L., Yang, Y., et al. 2016. Apparent gas permeability in an organic-rich shale reservoir. *Fuel* **1**(181):973–984.

Sparreboom W., Berg, A., and Eijkel, J.C.T. 2009. Principles and applications of nanofluidics transport. *Nat Nanotechnol* **4**(11): 713—720.

Sun, Y., and Chan, W.K. 2003. Analytic modeling of ultra-thin-film bearings. *J Micromech Microeng* **13**:463–473.

Tran, H., and Sakhaee-Pour, A. 2016. Viscosity of shale gas. *Fuel* **191**:87–96.

Veijola, T., and Turowski, M. 2001. Compact damping models for laterally moving microstructures with gas-rarefaction effects. *J Microelectromech Syst* **10**(2):263–273.

Washburn, E.W. 1921. The dynamics of capillary flow. *Phys Rev* **17**:273–283.

Yu, W., Lashgari, H.R., Wu, K., and Sepehrnoori, K. 2015. CO_2 injection for enhanced oil recovery in Bakken tight oil reservoirs. *Fuel* **159**:354–363.

Appendix A

The appendix contains the full-length article submitted to the Fuel journal, Viscosity of shale Gas (Tran and Sakhaee-Pour, 2017).

Fuel 191 (2017) 87–96

Contents lists available at ScienceDirect

Fuel

journal homepage: www.elsevier.com/locate/fuel

Full Length Article

Viscosity of shale gas

Huy Tran, A. Sakhaee-Pour *

Petroleum and Geological Engineering, The University of Oklahoma, USA

HIGHLIGHTS

- Effective gas viscosity of a shale using a physically representative pore model.
- Effects of a pressure change on the effective gas viscosity.
- Practical implications of permeability measurements for shale gas viscosity.
- Practical applications of the effective gas viscosity for a reservoir model.

ARTICLE INFO

Article history:
Received 14 September 2016
Received in revised form 7 November 2016
Accepted 16 November 2016
Available online 24 November 2016

Keywords:
Shale
Effective gas viscosity
Acyclic pore model

ABSTRACT

Nanofluidics, which analyzes fluid transport through sub 100-nm conduits, has fascinated engineers in different fields and we petroleum engineers are no exception. This field gained a significant interest in petroleum engineering only when hydrocarbon production from shales became economically feasible. The basic transport properties of the fluid change for this range of conduit size. With this in mind, we analyze the effective gas viscosity of a shale at different pore pressures. Our objective is not to derive detailed information about the gas transport at a pore or a sub-pore scale, but rather to discuss the implications of pore-scale simulations on the effective gas viscosity at the core scale. We use an acyclic pore model to account for the effective connectivity of the pore space at the core scale. The acyclic model is physically representative because it can capture capillary pressure measurements of the drainage obtained from mercury intrusion experiments. We present the effective gas viscosity with respect to the nominal value, under unconfined conditions. Our analysis shows that the reported permeability in a pressure-driven flow has to be considered an effective transport property if nominal viscosity and density are used for interpretation. That is, we have to modify viscosity and permeability simultaneously in our reservoir model. Our study has major implications for building a realistic reservoir model for shales based on petrophysical measurements.

1. Introduction

Hydrocarbon production from shale formations, which became economically feasible due to hydraulic fracturing, launched a new era in petroleum industry with major implications. The implications were relevant to and significant for a wide range of issues, including research conducted in petroleum engineering. For the first time, researchers with petroleum engineering backgrounds began analyzing hydrocarbon flow in a porous medium whose characteristic pore-throat sizes are usually smaller than 100 nm. This is the advent of nanofluidics in petroleum engineering, as a better understanding of transport in sub-100-nm conduits is important not only scientifically but also has practical and economic consequences.

Recent studies have successfully coupled a borehole flow model with production logs to determine the relative permeability of a formation [1,2]. The coupled model is unique in that the effective transport properties were derived at a large scale that are not possible to measure directly in the lab. Other studies accounted for the pore structure effect to determine the transport properties of a shale [3–6], which can be significantly different from those of highly-permeable formations. The notable difference could be due to the smaller pore-throat size and the inferior pore connectivity. The smaller pore-throat size leads to fundamental changes in transport properties at the pore scale, such as density and viscosity [7]. Further, it has an impact on the flow conductance, which in turns alters the permeability [8–10]. With the importance of the

* Corresponding author.
E-mail address: sakhaee@ou.edu (A. Sakhaee-Pour).

http://dx.doi.org/10.1016/j.fuel.2016.11.062
0016-2361/

pore connectivity in mind, many researchers have also analyzed the pore structure of a shale [11–13].

Nanofluidics is the study and application of fluid flow in channels and pores whose characteristic sizes are below 100 nm [14,15]. This definition includes hydrocarbon transport in the matrix of a shale formation because of its characteristic pore-throat size [8]. The fluid behavior changes significantly when we go from the macroscale, or even the microscale, to the nanoscale [16]. One of the main reasons for the difference between these behaviors is that the distance between the molecules becomes comparable to the size at which the relevant properties are evaluated. This implies that the assumption of a continuous medium is no longer realistic—that is, it is not realistic to model fluids, both in the liquid and in the gas phases, as continua. The relevant transport properties, such as the viscosity and density, of fluids that are confined in a nano-size channel are different from those reported at ambient conditions.

Many researchers analyzed the transport properties of shales at the pore scale, which are different from those reported at ambient conditions. The conducted investigations allow us to model the density variation inside a single pore [17,18,19] and how hydrocarbon can form an adsorbed layer [20]. Kazemi and Takbiri-Borujeni [21] accounted for these phenomena by simulating gas displacement inside a single conduit. While these studies shed light on the complexity of modeling mass transport in shales, it remains difficult to relate them to the effective transport properties at the core scale. Relating the fundamental changes of the transport properties at the pore scale to those of the large scale entails a representative model for the pore space at the core scale.

There is one fundamental difference between the pore space of a shale formation and artificially built conduits in typical nanofluidic devices: the pore space possesses more complicated geometries, as they are formed in nature. This implies that our knowledge of nanofluidics, and even microfluidics, is not applicable to porous media such as shales unless we account for the interconnectivity of the pores inside the pore space at a scale of interest.

There are few theoretical pore models that account for the effective connectivity of the pore space at the core scale [22–26]. The core scale is relevant to the size of a core, which is usually on the order of few centimeters. In theoretical pore models, we hypothesize a spatial distribution for the pore throats relative to each other a priori, and then test whether the adopted distribution is consistent with lab measurements. This is different from pore models that are based on high-resolution images [27,28] because there is no prior assumption regarding the effective connectivity of the pore space at the large scale in those models, and the pore space is extracted from the images.

Washburn [22] invented the theoretical pore model when he supposed that a bundle of tubes could capture the effective connectivity of the pore space. Subsequently, Purcell [29] used the bundle-of-tubes model to predict single-phase flow rate through porous media. Fatt [23] improved such modeling significantly by accounting for the interconnectivity of the pores; he showed that it is possible to capture the transport properties of the pore space using a regular-lattice model. Another theoretical approach that accounted for the interconnectivity of the pores was based on the premise that spheres, or beads, can represent the grains of a sedimentary rock, and thus the empty spaces between them can mimic the void space [24,30,31].

Sakhaee-Pour and Bryant [25] indicated that the multi-type model can capture the effective connectivity of the pore space in tight gas sandstones. A porous medium is considered tight when its matrix permeability is smaller than or equal to 10 microdarcy. The multi-type model comprises a lattice model and a tree-like model [32] that mimic the intergranular (between the grains) and intragranular (within the grains) void spaces, respectively. Mousavi and Bryant [33] showed that it is impossible to capture two-phase flow in tight gas sandstones if we use only a spatially random distribution of the pore-throat size due to the topology of the void space (its spatial distribution) and not to the pore-throat sizes, as the researchers picked the pore-throat sizes to be representative of the measurements.

Different groups modeled single-phase flow in a shale formation using a single channel [34] and a network of connected conduits [9,35,36]. Sakhaee-Pour and Bryant [26] suggested that the acyclic pore models can capture the effective connectivity of the pore space in shales. The pore model is acyclic in a graph theoretic sense [32]. More recently, Sakhaee-Pour and Li [37] indicated that the pore space of a shale formation can also follow the general scaling rules of a fractal. The acyclic pore model also has applications in geothermal reservoirs [38,39].

In the present study, we first review viscosity models for gas flow inside a single conduit. We then determine the effective gas viscosity for a single conduit whose characteristic size is relevant to shale formations. Later, we use the acyclic pore model to represent the pore space of a shale formation and calculate the effective viscosity. We discuss how the reported lab measurements can help us build a more realistic model for shales at in-situ conditions in the light of the presented results.

2. Gas viscosity for a single conduit

Our objective here is to determine how gas viscosity inside a single nano-size conduit is different from the nominal value at identical pressures and temperatures. We will use the results subsequently in a pore-scale model. We begin with the Knudsen number (Kn) definition, which allows us to predict different transport properties by determining the flow regime, as follows [40]:

$$Kn = \frac{\mu_{nominal}}{\rho D}\sqrt{\frac{\pi m}{2k_B T}} \tag{1}$$

where Kn is the Knudsen number, $\mu_{nominal}$ is the nominal gas viscosity under unconfined conditions (outside of a conduit), ρ is the gas density, D is the conduit diameter, m is the gas molecular mass, k_B is the Boltzmann constant, and T is the thermodynamics temperature.

Researchers have proposed different models for predicting the gas viscosity inside a single conduit. We present the results in the ratio form as a function of the Knudsen number (Kn) as follows:

$$\frac{\mu_{tube}}{\mu_{nominal}} = C(Kn) \tag{2}$$

where μ_{tube} is the gas viscosity inside the conduit, $\mu_{nominal}$ is the nominal viscosity of the gas at identical pressures and temperatures outside of the conduit, and $C(Kn)$ is the rarefaction coefficient defined for a single conduit. Table 1 lists various models for the rarefaction coefficient available in the literature.

The rarefaction coefficients in Table 1 relates the effective viscosity to the nominal viscosity by accounting for the conduit size, gas density, and temperature, which are implemented in the Knudsen number (Eq. (1)). The provided models are based on the assumption that the gas has a minimum affinity to the pore wall. Thus, the listed coefficients are more realistic when the void space is inside an inorganic material. When gas flow takes place inside an organic material, similar to Barnett shale, the effect of a minerology has to be implemented for gas transport [9,48,49]. The main conclusion of our study, which is that the viscosity and permeability cannot be measured independently, does not change even if the effect of the minerology is included in the rarefaction coefficient.

Now, we evaluate the importance of the conduit size to the effective viscosity, which we will use to build a physically representative pore model. For this reason, we determine the ratio of

Table 1
Existing models for the rarefaction coefficient, $C(Kn)$, which allows us to relate the gas viscosity inside a single conduit to the nominal value.

Model	$C(Kn)$	Fitting parameters	Range	Reference
1	$\frac{1.30\,56Kn^2+2\pi Kn}{1.30\,56Kn^2+7.59\,39Kn+\pi^2} \times \left(\frac{1}{2}+\alpha_m Kn\right)$	$\alpha_m = \beta_0 + \beta_1 \tan^{-1}(\beta_2 Kn^{\beta_3})$ $\beta_0 = 1.2977$ $\beta_1 = 0.71851$ $\beta_2 = -1.17488$ $\beta_3 = 0.58642$	$0 < Kn < 12$	Cercignani [41]
2	$\frac{1.270042\pi}{2(1+2.222Kn)} \left(\frac{1}{2}+\alpha_m Kn\right)$	$\alpha_m = \beta_0 + \beta_1 \tan^{-1}(\beta_2 Kn^{\beta_3})$ $\beta_0 = 1.2977$ $\beta_1 = 0.71851$ $\beta_2 = -1.17488$ $\beta_3 = 0.58642$	$0 < Kn < 12$	Sone et al. [42]
3	$\frac{1}{1+2Kn+0.2Kn^{0.788}e^{-\frac{1}{10}}}$	—	$0 < Kn < 1$	Veijola [43]
4	$\frac{0.529669Kn+1.20597}{0.529669Kn^2+1.627666Kn+0.602985} \times \left(\frac{1}{2}+\alpha_m Kn\right)$	$\alpha_m = \beta_0 + \beta_1 \tan^{-1}(\beta_2 Kn^{\beta_3})$ $\beta_0 = 1.2977$ $\beta_1 = 0.71851$ $\beta_2 = -1.17488$ $\beta_3 = 0.58642$	$0 < Kn < 12$	Bahukudumbi et al. [44]
5	$\frac{1}{1+2Kn}$	—	$0.1 < Kn < 10$	Sun and Chan [45]
6	$\frac{1}{1+2.2Kn}$	—	$0.1 < Kn < 10$	Karniadakis et al. [46]
7	$\frac{1+6Kn-6Kn^2}{1+6K_n+13.5Kn^2}$	—	$0 < Kn < 0.25$	Roohi-NS [47]
8	$\frac{1+0.89Kn+4.704Kn^2}{1+0.75Kn+19.98Kn^2}$	—	$0.1 < Kn < 0.5$	Roohi-IP [47]

the conduit viscosity to the nominal value using different models (function $C(Kn)$ in Eq. (2)). We present the results for relatively high and low pressures that are relevant to the early life of a well and after substantial gas production, respectively.

Figs. 1a and 1b exhibit the ratio of the effective gas viscosity for a single conduit to the nominal value at 500 and 5000 psi, respectively. The ratio increases and becomes closer to unity with an increase in the conduit size because the flow behavior becomes more similar to that of the continuum flow based on the Knudsen number (Kn). The Knudsen number is inversely proportional to the conduit size (Eq. (1)). The ratio of the viscosities increases from 0.86 to 0.99 at 5000 psi when the conduit size varies between 3.6 and 20 nm, which is typical for a shale. Hence, the effective viscosity of the gas inside the conduit is close to that of the unconfined conditions at an early period of production, regardless of the pore-throat size. The ratio becomes much smaller and reduces to 0.3 at the lower pressure (Fig. 1b). The deviation from the nominal value is more important during a later period of production.

Next, we determine the effect of the fluid pressure on the effective gas viscosity for a single conduit. We analyze the results for 2-nm and 20-nm conduits shown in Figs. 2a and 2b, respectively. The ratio becomes close to unity at high pressures, which means gas behaves in a manner more similar to a continuum medium. This is because of the dependency of the Kn on the pressure, whose effect mitigates the effect of the small conduit size (Eq. (1)). For a 2-nm conduit, the deviation from the nominal value becomes significant even at relatively high pressures: for instance, the ratio is close to 0.5 at 2000 psi in some models. The deviation from the nominal value is less significant for the wider conduit; compare Fig. 2b with 2a.

3. Methodology

3.1. Pore-scale model

We use the tree-like pore model [26], which is an acyclic pore model, to characterize the pore space. There is a unique path between any two points in the tree-like model [32] when they are connected (Fig. 3a). The main feature of the tree-like pore model as it relates to our analysis is that the accessibility of wider pores is not restricted by narrower pores; that is, narrower pores are accessible from wider throats. The tree-like pore model can capture the drainage experiment when the variation of the capil-

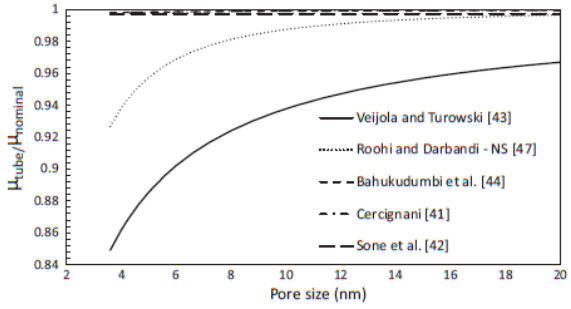

Fig. 1a. Ratio of the effective gas viscosity to the nominal viscosity inside a single conduit at a high pressure (5000 psia), which is more representative of an early period of production. The deviation from the nominal value increases with decreasing the conduit size, but the difference remains mainly negligible.

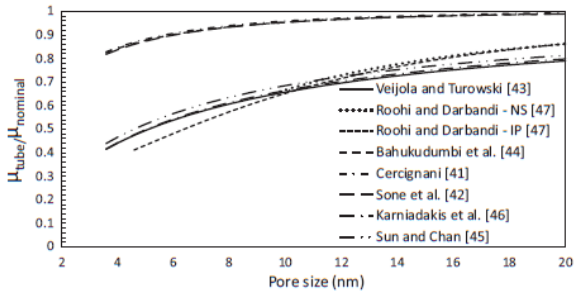

Fig. 1b. Ratio of the effective gas viscosity to the nominal viscosity inside a single conduit at a low pressure (500 psia), which is more representative of a later period of production. The deviation from the nominal value is significant and increases with decreasing pore-throat size.

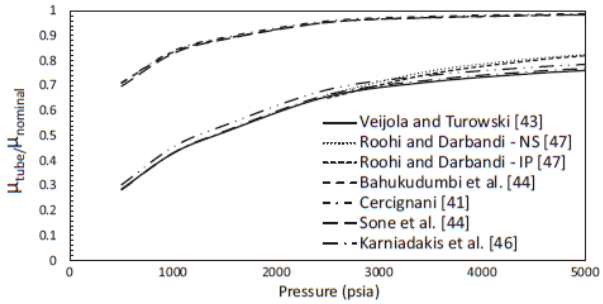

Fig. 2a. Ratio of the effective gas viscosity inside a 2-nm conduit at different pressures. The deviation from the nominal value is significant even at relatively high pressures based on some models.

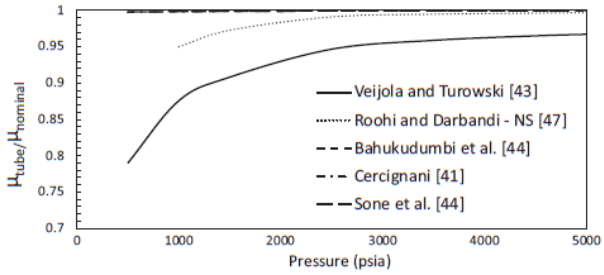

Fig. 2b. Ratio of the effective gas viscosity inside a 20-nm conduit at different pressures. The deviation from the nominal value remains relatively negligible unless pressure drops below 1000 psi.

lary pressure with wetting phase saturation exhibits a non-plateau-like trend (Fig. 3b).

We can determine the corresponding permeability of each conduit size to characterize the pore space. The no-slip permeability for the creeping flow can be calculated as follows:

$$k_{tube} = \frac{\varphi D^2}{32} \tag{3}$$

where k_{tube} is the permeability of the porous medium that includes conduits with similar sizes, D is the corresponding conduit size, and φ is the porosity of the sample.

We can also compute the total cross-sectional area of the conduits whose characteristic sizes are equal. These conduits are invaded at an equal capillary pressure during drainage. The total cross-sectional area is a strong function of the incremental pore volume invaded at each capillary pressure, which we can determine as follows:

$$A_i L_i = V_p \Delta S_{wi} \tag{4}$$

where A_i is the total cross-sectional area of the conduits invaded at the capillary pressure increment i, L_i is the corresponding total length of the conduits invaded at the corresponding capillary pres-

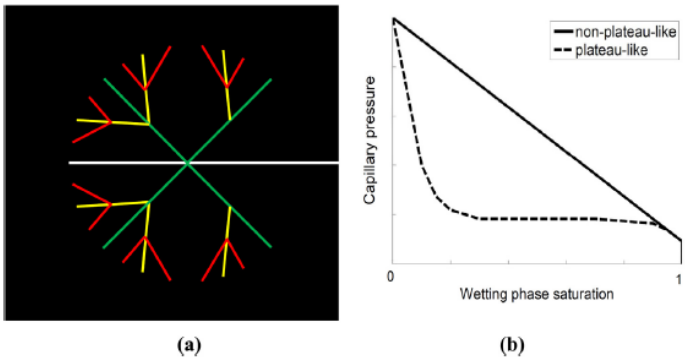

Fig. 3. (a) Tree-like pore model in which there is a single path between any two points in the model [32] and narrower pores do not limit the accessibility of wider pores. The red color represents the narrowest conduit and the white color the widest conduit. (b) The tree-like pore model is physically representative of the pore space when a non-plateau-like trend is observed in capillary pressure measurements [26]. (For interpretation of the references to colour in this figure legend, the reader is referred to the web version of this article.)

sure, ΔS_{wf} is the corresponding change in the wetting phase saturation at that capillary pressure, and V_p is the pore volume of the rock. For simplicity, we take the length of the widest throat to be equal to the length of the sample and we assume the ratio of the lengths of the conduits at sequential pressures is a constant value (=branching ratio). The branching ratio does not have to be a constant number for the pore model, but this assumption allows us to simplify the redundant complexities of the model, which do not affect the main conclusion of this study.

3.2. Effective viscosity of a pore-scale model

We determine the effective viscosity for a pressure-driven flow, as opposed to shear-driven flow such as Couette flow, simply because it is more relevant to transport in petroleum engineering. We first elaborate the effective permeability calculation for the tree-like pore model because it is closely coupled with the effective viscosity in a pressure-driven flow. For this reason, we suppose that the fluid flow takes place from a porous medium, which is at a higher pressure relative to outside. Fig. 4a shows a schematic of the fluid flow where the line thickness represents the pore-throat size. The pressure distribution diagram for the flow patterns is provided in Fig. 4b.

Following the flow path from a higher pressure to a lower pressure in each branch ($P_1 \rightarrow P_2$, $P_2 \rightarrow P_3$, and $P_3 \rightarrow P_{out}$) allows us to determine the permeability. The pore model is the combination of conduits that act in parallel and in series. The narrowest conduit acts in parallel with a portion of the wider conduit that connects identical pressures (P_1 and P_2 in Fig. 4b). Their outcome acts in series with the remainder of the wider conduit that connects P_2 to P_3. This spatial distribution allows us to derive the effective permeability for the two narrowest conduits as follows:

$$(k_{e-p})_{1\rightarrow 2}(A_{e-p})_{1\rightarrow 2} = k_1 A_1 + k_2 A_2 \tag{5}$$

where $(k_{e-p})_{1\rightarrow 2}$ is the effective permeability of the pore-scale model between P_1 and P_2 containing the two narrowest conduits and $(A_{e-p})_{1\rightarrow 2}$ is the corresponding effective area. We use subscript p when the derived parameter is for media that act in parallel and s when they act in series. k_1 is the corresponding permeability of the smallest pore-throat size (Eq. (3)) and A_1 is the corresponding total cross-sectional area (Eq. (4)). k_2 and A_2 are relevant to the second smallest pore-throat size.

The effective medium, whose permeability is calculated in Eq. (5), acts in series with the remainder of the wider conduits stretched between P_2 and P_3. Thus, we can determine the effective

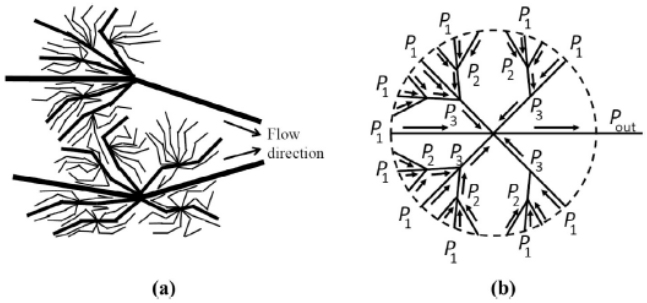

Fig. 4. (a) Schematic of flow patterns from the porous medium, whose pore pressure is higher than the outside pressure. (b) Pressure distribution diagram for the flow patterns.

permeability and the cross-sectional area of the two narrowest sizes as follows:

$$\frac{L_{1\to3}}{(k_{e-s})_{1\to3}(A_{e-s})_{1\to3}}=\frac{L_{1\to2}}{(k_{e-p})_{1\to2}(A_{e-p})_{1\to2}}+\frac{L_{2\to3}}{k_2A_2} \tag{6}$$

where $L_{1\to3}$ is the length of Conduit 2 between P_1 and P_3, $L_{1\to2}$ is the length of Conduit 1 between P_1 and P_2, and $L_{2\to3}$ is the length of Conduit 2 between P_2 and P_3 ($L_{1\to3}=L_{1\to2}+L_{2\to3}$). The pore-throat size of a conduit increases with its number; that is, Conduit 1 is the narrowest conduit and Conduit 2 is the second narrowest conduit in the acyclic model. We denote the effective permeability of the pore-scale model that contains Conduits 1 and 2 between P_1 and P_3 by $(k_{e-s})_{1\to3}$ and its corresponding cross sectional area by $(A_{e-s})_{1\to3}$.

We repeat this process to find the effective permeability of the pore-scale model. This is an iterative process in which the effective permeability of parallel and series combinations are used for each other. The effective permeability can be calculated as follows:

$$(k_{e-p})_{1\to j}(A_{e-p})_{1\to j}=(k_{e-s})_{1\to j}(A_{e-s})_{1\to j}+k_jA_j \quad j=3 \text{ to } n \tag{7}$$

$$\frac{L_{1\to j}}{(k_{e-s})_{1\to j}(A_{e-s})_{1\to j}}=\frac{L_{1\to j-1}}{(k_{e-p})_{1\to j-1}(A_{e-p})_{1\to j-1}}+\frac{L_{j-1\to j}}{k_{j-1}A_{j-1}} \quad j=4 \text{ to } n \tag{8}$$

where n is the number of pore-throat sizes, which is equal to the number of capillary pressure measurements. The number of capillary pressure measurements, which is equal to 17 in our study, is usually on the order of 10–100 [50]. $(k_{e-p})_{1\to j}$ is the effective permeability of the pore-scale model between P_1 and P_j and $(A_{e-p})_{1\to j}$ is the corresponding effective area, $(k_{e-s})_{1\to j}$ is the effective permeability of the pore-scale model that contains Conduit 1 and Conduit $(j-1)$ between P_1 and P_j and $(A_{e-s})_{1\to j}$ is the corresponding effective area. $L_{1\to j}$ is the closest distance between P_1 and P_j, $L_{1\to j-1}$ is the closest distance between P_1 and P_{j-1}, and $L_{j-1\to j}$ is the closest distance between P_{j-1} and P_j in the model. The permeability values calculated here are nominal and relevant to no-slip boundary conditions. We find the nominal permeability of the pore-scale model when j becomes equal to n.

Now, we turn to the effective viscosity calculation by eliminating the permeability effect. This is basically a weighted average of the gas viscosity inside the pore-scale model. Similar to the effective permeability calculation, we follow the flow path from the higher pressure to the lower pressure. The gas viscosity is dependent on the Kn (Eq. (2)), in contrast to the nominal permeability calculation. Thus, we can no longer discard the viscosity terms from the mass balance equation of the pore-scale model. Considering that the narrowest conduits act in parallel with part of the wider conduit that connects identical pressures (P_1 and P_2), we can calculate the effective viscosity as follows:

$$\frac{1}{(\mu_{e-p})_{1\to2}}=\frac{1}{(k_{e-p})_{1\to2}(A_{e-p})_{1\to2}}\left(\frac{k_1A_1}{\mu_{tube-1}}+\frac{k_2A_2}{\mu_{tube-2}}\right) \tag{9}$$

where $(\mu_{e-p})_{1\to2}$ is the effective viscosity of fluid flow inside Conduits 1 and 2, μ_{tube-1} is the gas viscosity inside Conduit 1, and μ_{tube-2} is the gas viscosity inside Conduit 2. We can express the ratio of the effective viscosity to the nominal value to define the effective rarefaction coefficient as follows:

$$(C_{e-p})_{1\to2}=\frac{(\mu_{e-p})_{1\to2}}{\mu_{nominal}}=\frac{(k_{e-p})_{1\to2}(A_{e-p})_{1\to2}}{\frac{k_1A_1}{C_1(Kn)}+\frac{k_2A_2}{C_2(Kn)}} \tag{10}$$

where $(C_{e-p})_{1\to2}$ is the effective rarefaction coefficient for the gas phase between P_1 and P_2 through Conduits 1 and 2, and C_1 and C_2 are the corresponding rarefaction coefficients.

The effective medium acts in series with the remainder of the wider conduits stretched between P_2 and P_3. Thus, we can determine the effective rarefaction coefficient as follows:

$$(C_{e-s})_{1\to3}=\frac{(\mu_{e-s})_{1\to3}}{\mu_{nominal}}=\frac{(k_{e-s})_{1\to3}(A_{e-s})_{1\to3}}{L_{1\to3}}\left(\frac{(C_{e-p})_{1\to2}L_{1\to2}}{(k_{e-p})_{1\to2}(A_{e-p})_{1\to2}}+\frac{C_2L_{2\to3}}{k_2A_2}\right) \tag{11}$$

where $(C_{e-s})_{1\to3}$ is the effective rarefaction coefficient for gas flow between P_1 and P_3 through conduits 1 and 2 whose effective viscosity is represented by $(\mu_{e-s})_{1\to3}$.

The calculation of the effective rarefaction coefficient of the pore-scale model is an iterative process similar to the effective permeability calculation. We repeat the calculation of the effective rarefaction coefficients of the media that act in series and in parallel to determine the effective viscosity of the pore-scale model as follows:

$$(C_{e-p})_{1\to j}=\frac{(\mu_{e-p})_{1\to j}}{\mu_{nominal}}=\frac{(k_{e-p})_{1\to j}(A_{e-p})_{1\to j}}{\frac{(k_{e-s})_{1\to j-1}(A_{e-s})_{1\to j-1}}{(C_{e-s})_{1\to j-1}}+\frac{k_{j-1}A_{j-1}}{C_{j-1}}} \quad j=3 \text{ to n} \tag{12}$$

$$(C_{e-s})_{1\to j}=\frac{(\mu_{e-s})_{1\to j}}{\mu_{nominal}}=\frac{(k_{e-s})_{1\to j}(A_{e-s})_{1\to j}}{L_{1\to j}}\left(\frac{(C_{e-p})_{1\to j-1}L_{1\to j-1}}{(k_{e-p})_{1\to j-1}(A_{e-p})_{1\to j-1}}+\frac{C_{j-1}L_{j-1\to j}}{k_{j-1}A_{j-1}}\right) \quad j=4 \text{ to n} \tag{13}$$

where $(C_{e-p})_{1\to j}$ and $(C_{e-s})_{1\to j}$ are the effective rarefaction of the media when they act in parallel and in series, respectively, and n is the number of conduit sizes used. The effective rarefaction of the pore-scale model is equal to $(C_{e-s})_{1\to j}$ when j becomes equal to the number of pore-throat sizes (n).

4. Results

In the present study, we determine the effective viscosity of a shale gas. Our objective is not to derive detailed information about the gas transport at the pore or sub-pore scale, but rather to determine the effects of viscosity deviation from the nominal value at the core scale. We use mercury intrusion capillary pressure measurements because they are representative of the connected pore space at the core scale. We do not interpret the pore space based on high-resolution images because it is not yet possible to extract a pore model that is representative of the core scale based on such images. The high-resolution images are acquired with no confinement and are not necessarily representative of in-situ conditions. Some micro-cracks that are open in these images are closed at subsurface conditions.

We use the drainage data (Fig. 5) obtained using mercury intrusion under confined boundary conditions [13]. The wetting phase saturation (S_w) is based on the mercury saturation (S_{Hg}) measured during the test ($S_w=1-S_{Hg}$). The invasion begins when the capillary pressure is almost equal to 15,000 psi and the capillary pressure increases almost linearly with decreasing nonwetting phase saturation. The linear increase of the capillary pressure with the decreasing wetting phase saturation is consistent with the tree-like pore model [26].

The pore-throat size distribution used in our study is obtained from mercury intrusion capillary pressure measurements conducted on a core plug (Fig. 5). Thus, they are representative of the effective connectivity of the pore space at the core scale. The measurements were conducted under confined boundary conditions, which close microfractures, at least partially.

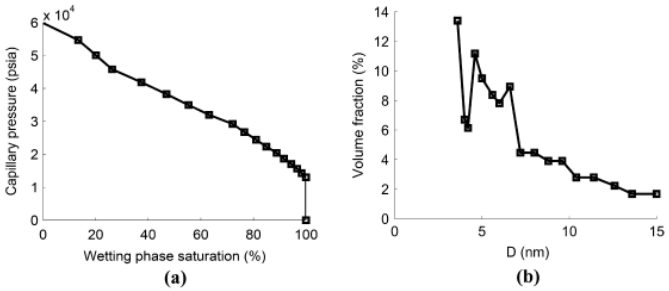

Fig. 5. (a) Capillary pressure measurements [13] of a shale sample that is used for effective viscosity calculation. The absence of the plateau-like trend indicates that the tree-like pore model can capture the effective connectivity of the pore space at the core scale [26]. (b) Pore-throat size distribution of the sample is determined using the Young-Laplace relation.

The deviation of the effective viscosity from the nominal value becomes more significant when the conduit size decreases (Fig. 1). In our study, the largest pore-throat size is on the order of 15 nm (Fig. 5), which implies that the void space corresponds to the matrix of a formation. The average pore-throat size increases when there are open micro fractures. Hence, our analysis is relevant to the condition where the deviation from a nominal value is more significant, by including ultra-narrow throats.

Now, we calculate the effective viscosity of the shale sample using the pore-scale model. We first determine the effect of the branching ratio on the effective viscosity at high and low pressures. We compute the effective viscosity using the two models that provide the upper and lower bounds based on our analysis for the gas viscosity of a single conduit [43,44]. Fig. 6 reveals that the effective viscosity is not a function of the branching ratio. While the branching ratio changes the topology of the pore-scale model significantly, its impact on the effective viscosity is insignificant.

Next, we turn to the dependency of the effective viscosity on the pore pressure. We determine the effective viscosity for the two branching ratios (Fig. 7) because they do not play an important role (Fig. 6). For a typical pore-throat size relevant to a shale formation (Fig. 5b), the Knudsen number (Kn) is on the order of 0.15–0.64 when the pore pressure is 500 psia, and it varies between 0.02 and 0.08 when the pressure becomes equal to 5000 psia. The ratio of the effective viscosity to the nominal viscosity remains larger than or equal to 0.9 when the pore pressure is larger than or equal to 2000 psi. The ratio decreases with decreasing pore pressure but remains larger than 0.75 when the pore pressure varies between 2000 and 500 psi. Thus, the difference between the effective viscosity and the nominal viscosity is negligible at an early period of production. The deviation from the nominal value is relatively important only at a late period of production because of the increase in the Kn, mainly due to a decline in density.

Fig. 7 reveals that the smallest ratio is close to 0.73 based on the acyclic pore model. The smallest ratio (0.73) lays between the smallest ratio corresponding to a 20-nm conduit (0.78) and a 2-nm conduit (0.28) shown in Fig. 2. This tells us that the effective viscosity is controlled mainly by wider conduits. We determine the effective pore-throat size, which dominates the effective viscosity subsequently (Fig. 8).

Last, we determine the pore-throat size corresponding to the effective viscosity of the pore-scale model (Fig. 8). This might be interpreted as the pore-throat size that controls the effective viscosity (effective pore-throat size). Prediction of the effective pore-throat size could have major implications for understanding hydrocarbon transport in shales when we do not want to build a pore-scale model. Again, we use the two models that yield the upper and lower bounds for the effective viscosity. The branching ratio is set equal to 2 because its effect on the effective viscosity is negligible. Fig. 8 reveals that the effective pore-throat size is

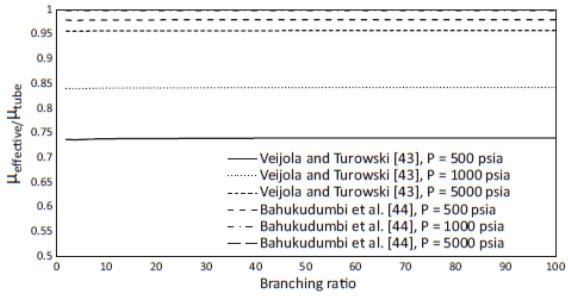

Fig. 6. Effect of the branching ratio on the ratio of the effective viscosity to the nominal viscosity is negligible. We use only the two models that provide upper and lower bounds for the effective viscosity.

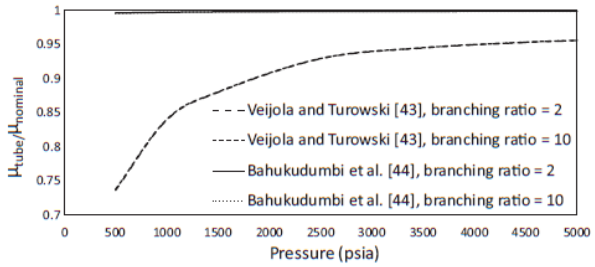

Fig. 7. Ratio of the effective viscosity to the nominal viscosity as a function of pore pressures with two branching ratios for the two models that provide the upper and lower bounds for the effective viscosity.

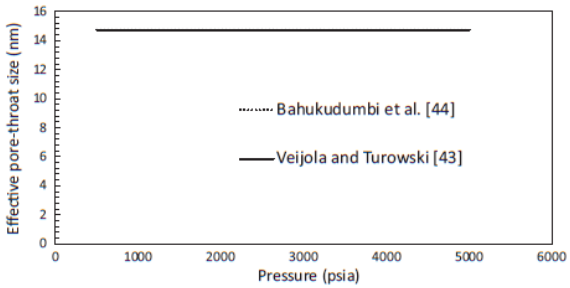

Fig. 8. Effective pore-throat size, whose corresponding effective viscosity is equal to the effective viscosity of the pore-scale model, is almost equal to the largest pore-throat size included in the tree-like pore model. The branching ratio is set equal to 2 here for the effective pore-throat size calculation because it plays a negligible role.

almost equal to the largest size reported based on the drainage, and is independent of the pore pressure. This is because of the topology of the tree-like pore model. At a given pore pressure, the Knudsen number (Kn) takes the smallest value in the widest conduits (Eq. (1)) that leads to the largest gas viscosity for the widest conduits. The largest viscosity results in a higher resistance against the flow that is important at the pore-scale because it acts in series with remainder of the pore space. This does not necessarily mean that the effective transport properties of the wider pores are inferior in a nanofluidic system because we only analyze the effective viscosity and not the overall transport.

The network modeling approach used in this study has been tested against different lab measurements. First, Sakhaee-Pour and Bryant [9] used the network modeling approach to predict gas permeability for different pore pressures. They accounted for the combined effects of an adsorbed layer and slippage on the flow conductance of a single conduit. They then related the results to the transport properties of a core plug by taking into account the interactions among the pores. They tested the results against lab measurements.

Sakhaee-Pour and Bryant [26] subsequently used the network modeling approach to capture the no-slip permeability of a shale formation based on mercury intrusion capillary pressures, which allowed them to develop the acyclic pore model. The predicted results were compared with reported no-slip permeability. More recently, Sakhaee-Pour and Li [37] showed that the acyclic pore model can not only capture the capillary pressures measurements of a shale but also can characterize its fractal properties relevant to pore-throat and pore-body sizes.

5. Discussion

The dependency of the viscosity on the conduit size is an intrinsic characteristic of a nanofluidic system, which is relevant to shales because their pore-throat sizes are usually smaller than 20 nm. The dependency becomes insignificant in more permeable formations because of their wider pores. There are different sizes associated with each pore, such as pore-throat size and pore-body size. The pore- throat size is more relevant to the flow resistance between neighboring pores, as opposed to the pore-body size; hence, we used the pore-throat size obtained from drainage in our study.

The gas viscosity is predicted based on the Knudsen number (Kn), which is proportional to the inverse of the characteristic size (Eq. (1)). The viscosity deviation from the nominal becomes more significant when this dimensionless number increases. Thus, using pore-throat size, which is the narrowest region of a pore for a given pressure and temperature, allowed us to determine the effect of viscosity change when its deviation from the nominal value is maximum. Based on our analysis, the effect of such deviation on the effective transport properties at the core scale is negligible. The deviation from the effective core-scale properties is even less significant if we use other characteristic sizes of a pore.

To determine the effective viscosity, we presented the results with respect to the nominal permeability. We did not account for the shale gas compressibility, which is different from the value used in conventional reservoirs with large pores. The compressibility value depends on the pore size in a shale formation because the pore pressure does not change significantly at the core scale in a

single-phase flow. The determined viscosity remains an effective transport property, similar to the permeability, if it is based on the interpretation of lab measurements with nominal values. The interpretation of lab measurements for effective viscosity was the main objective of our study, which was a thought experiment.

5.1. Practical implication

The gas viscosity inside a nano-size conduit is lower than the nominal value. The lower viscosity enhances the flow rate, whose effect is similar to that of slippage. We were able to differentiate the viscosity effect because the viscosity models in the literature are reported for a shear-driven flow, as opposed to a pressure-driven flow. It is impossible to distinguish the viscosity and the slippage effects based only on pressure driven measurements based on the nature of Hagen-Poiseuille or Darcy's equation. Thus, the permeability values reported based on lab measurements also embrace the viscosity effect and should be considered effective transport properties, rather than permeability values, when we use nominal values for viscosity and density. The practical implications of this are that we should not implement viscosity and permeability values separately in reservoir models if the permeability value is based on lab measurements with nominal parameters.

6. Conclusions

The characteristic pore-throat size of a shale formation is usually smaller than 20 nm, which classifies its pore space as a nanofluidic system. The basic transport properties inside nano-size conduits are different from the nominal values reported outside of the porous medium. With this in mind, we first determined the ratio of the effective viscosity to the nominal viscosity inside a circular conduit for methane (CH_4). We determined the gas viscosity inside a single conduit based on the Knudsen number (Kn). Our study for a single conduit shows the effective viscosity remains close to the nominal value at high pressure (~5000 psi), regardless of the pore-throat size. At low pressures (~500 psi), the ratio of the effective viscosity to the nominal value decreases to 0.2–0.7, based on different models.

We then adopted the tree-like pore model to account for the effective connectivity of the pore space at the core scale. The tree-like pore model interconnects the conduits in a manner similar to a tree's branches, which means there is a single path between any two points in the pore-scale model and narrower pores are accessible only from a wider pore. The model accounts for the effective connectivity of the pore space at the core scale by capturing capillary pressure measurements obtained from mercury intrusion. Our pore-scale model reveals that the effective viscosity of the pore-scale model is close to the corresponding value of the largest pore-throat size. The deviation from the nominal value is much less significant. This is mainly because of the topology of the tree-like pore model, where the widest pore acts in series with the remainder of the pore space, and plays a crucial role in controlling the transport properties.

The gas viscosity inside a nano-size conduit is smaller than the nominal value, which improves the flow rate in a manner similar to gas slippage. We were able to differentiate these effects because the viscosity models were based on shear-driven flow while the slippage is often accounted for in pressure-driven flows. It seems impossible to differentiate the effects of viscosity and slippage if we only analyze the pressure-driven flow, which is used for permeability measurements. Thus, the reported permeability in a pressure-driven flow has to be considered an effective transport property if nominal viscosity and density are used for interpretation. In other words, we have to modify viscosity and permeability simultaneously in our reservoir model for shale formations. This study has major implications for reservoir characterization based on standard lab measurements for shales.

References

[1] Frooqnia A, A-Pour R, Torres-Verdín C, Sepehrnoori K. Numerical simulation and interpretation of production logging measurements using a new coupled wellbore-reservoir model. Paper SPWLA VV. presented at the SPWLA 52nd international logging symposium, Colorado; 2011.

[2] Frooqnia A. Numerical simulation and interpretation of borehole fluid-production measurements Ph.D. dissertation. Austin, Texas (USA): The University of Texas at Austin; 2014.

[3] Yu W, Lashgari HR, Wu K, Sepehrnoori K. CO_2 injection for enhanced oil recovery in Bakken tight oil reservoirs. Fuel 2015;159:354–63.

[4] Ju B, Wu D. Experimental study on the pore characteristics of shale rocks in Zhanhua depression. J Petrol Sci Eng 2016;146:121–8.

[5] Ganjdanesh R, Rezaveisi M, Pope GA, Sepehrnoori K. Treatment of condensate and water blocks in hydraulic-fractured shale-gas/condensate reservoirs. SPE J 2016;21(2):665–74.

[6] Kadkhodaie A, Rezaee R. A new correlation for water saturation calculation in gas shale reservoirs based on compensation of kerogen–clay conductivity. J Petrol Sci Eng 2016;146:932–9.

[7] Ambrose RJ, Hartman RC, Diaz Campos M, Akkutlu IY, Sondergeld C. New pore-scale considerations for shale gas in place calculations. SPE Paper 131772. Presented at SPE unconventional gas conference. Pennsylvania; 2010.

[8] Javadpour F, Fisher D, Unsworth M. Nanoscale gas flow in shale gas sediments. J Can Pet Technol 2007;46(10).

[9] Sakhaee-Pour A, Bryant SL. Gas permeability of shale. SPE Reservoir Eval Eng 2012;15(04):401–9.

[10] Civan F, Devegowda D. Comparison of shale permeability to gas determined by pressure-pulse transmission testing of core plugs and crushed samples. SPE Paper 178571. Presented at SPE unconventional resources technology conference. Texas; 2015.

[11] Sondergeld CH, Ambrose RJ, Rai CS, Moncrieff J. Micro-structural studies of gas shales. Paper SPE 131771. Presented at the SPE unconventional gas conference. Pennsylvania; 2010.

[12] Tinni A, Sondergeld CH, Rai CS, Kouam H. Effective pressure and microstructure control on resistivity formation factor and seismic waves velocities. Paper SPE 147432. Presented at the SPE annual technical conference and exhibition. Colorado; 2011.

[13] Dewers TA, Heath J, Ewy R, Duranti L. Three-dimensional pore networks and transport properties of a shale gas formation determined from focused ion beam serial imaging. Int J Oil, Gas Coal Technol 2012;5(2–3):229–48.

[14] Eijkel JCT, Berg A. Nanofluidics: what is it and what can we expect from it? Microfluid Nanofluid 2005;1(3):249–67.

[15] Sparreboom W, Berg A, Eijkel JCT. Principles and applications of nanofluidic transport. Nat Nanotechnol 2009;4(11):713–20.

[16] Singh SK, Singh JK. Effect of pore morphology on vapor–liquid phase transition and crossover behavior of critical properties from 3D to 2D. Fluid Phase Equilib 2011;300(1–2):182–7.

[17] Ambrose RJ, Hartman RC, Diaz-Campos M, Akkutlu IY, Sondergeld C. Shale gas-in-place calculations Part I: new pore-scale considerations. SPE J 2012;17(1):219–29.

[18] Didar BR, Akkutlu IY. Pore-size dependence of fluid phase behavior and properties in organic-rich shale reservoirs. SPE Paper 164099, Presented at SPE international symposium on oilfield chemistry. Texas; 2013.

[19] Jadoon QK, Roberts E, Blenkinsop T, Wust RA, Shah SA. Petrophysical evaluation and uncertainty analysis of Roseneath and Murteree shales reservoirs in Cooper Basin, Australia (a case study). J Petrol Sci Eng 2016;146:330–45.

[20] Mosher K, He J, Liu Y, Rupp E, Wilcox J. Molecular simulation of methane adsorption in micro-and mesoporous carbons with applications to coal and gas shale systems. Int J Coal Geol 2013;109:36–44.

[21] Kazemi M, Takbiri-Borujeni A. Non-equilibrium molecular dynamics simulation of gas flow in organic nanochannels. J Natural Gas Sci Eng 2016;33:1087–94.

[22] Washburn EW. The dynamics of capillary flow. Phys Rev 1921;17:273–83.

[23] Fatt I. The network model of porous media. I. Capillary pressure characteristics. Pet Trans AIME 1956;207:144–81.

[24] Mellor DW. Random close packing (RCP) of equal spheres: structure and implications for use as a model porous medium PhD dissertation. UK: Open University; 1989.

[25] Sakhaee-Pour A, Bryant SL. Effect of pore structure on the producibility of tight-gas sandstones. AAPG Bulletin 2014;98(04):663–94.

[26] Sakhaee-Pour A, Bryant SL. Pore structure of shale. Fuel 2015;143:467–75.

[27] Blunt MJ, Bijeljic B, Dong H, Gharbi O, Iglauer S, Mostaghimi P. Pore-scale imaging and modelling. Adv Water Resour 2013;51:197–216.

[28] Mostaghimi P, Blunt MJ, Bijeljic B. Computations of absolute permeability on micro-CT images. Math Geosci 2013;45(1):103–25.

[29] Purcell WR. Capillary pressures-their measurement using mercury and the calculation of permeability therefrom. J Petrol Technol 1949;1(2):39–48.

[30] Finney J. Random packing and the structure of the liquid state PhD dissertation. London (UK): University of London; 1968.
[31] Bryant S, Cade C, Mellor D. Permeability prediction from geologic models. AAPG Bulletin 1993;77(8):1338–50.
[32] Bethe HA. Statistical theory of superlattices. Proc R Soc Lond A 1935;150 (871):552–75.
[33] Mousavi MA, Bryant SL. Connectivity of pore space as a control on two-phase flow properties of tight-gas sandstones. Transp Porous Media 2012;94 (2):537–54.
[34] Javadpour F. Nanopores and apparent permeability of gas flow in mudrocks (shales and siltstone). J Can Pet Technol 2009;48:16–21.
[35] Mehmani A, Prodanović M, Javadpour F. Multiscale, multiphysics network modeling of shale matrix gas flows. Transp Porous Media 2013;9 (2):377–90.
[36] Huang X, Bandilla KW, Celia MA. Multi-physics pore-network modeling of two-phase shale matrix flows. Transp Porous Media 2016;111(1):123.
[37] Sakhaee-Pour A, Li W. Fractal dimensions of shale. J Nat Gas Sci Eng 2016;30:578–82.
[38] Sakhaee-Pour A. Pore-scale modeling of The Geysers. Geothermics 2016;60:58–65.
[39] Sakhaee-Pour A. Fractality of the geysers. Geotherm Energy 2016;4(1):1–10.
[40] Knudsen M. The laws of molecular and viscous flow of gases through tubes. Ann Phys 1909;333(1):75–130.
[41] Cercignani C. Mathemathical methods in kinetic theory. 1st ed. US: Springer; 1969.
[42] Sone Y, Takata S, Ohwada T. Numerical analysis of the plane Couette flow of a rarefied gas on the basis of the linearized Boltzmann equation for hard-sphere molecules. Eur J Mech 1990;9:273–88.
[43] Veijola T, Turowski M. Compact damping models for laterally moving microstructures with gas-rarefaction effects. J Microelectromech Syst 2001;10(2):263–73.
[44] Bahukudumbi P, Park JH, Beskok A. A unified engineering model for steady and quasi-steady shear-driven gas microflows. Microscale Thermophys Eng 2003.
[45] Sun Y, Chan WK. Analytic modelling of ultra-thin-film bearings. J Micromech Microeng 2003;13:463–73.
[46] Karniadakis GE, Beskok A, Aluru N. Microflows and Nanoflows. Interdisciplinary Applied Mathematics. New York: Springer-Verlag; 2005.
[47] Roohi E, Darbandi M. Extending the Navier-Stokes solutions to transition regime in two-dimensional micro- and nanochannel flows using information preservation scheme. Phys Fluids 2009;21(8).
[48] Song W, Yao J, Li Y, Sun H, Zhang L, Yang Y, et al. Apparent gas permeability in an organic-rich shale reservoir. Fuel 2016;1(181):973–84.
[49] Wang S, Javadpour F, Feng Q. Fast mass transport of oil and supercritical carbon dioxide through organic nanopores in shale. Fuel 2016;1(181):741–58.
[50] Peters EJ. Advanced petrophysics: geology, porosity, absolute permeability, heterogeneity, and geostatistics. Greenleaf Book Group; 2012.